EurJIC
European Journal of Inorganic Chemistry

Full Papers
doi.org/10.1002/ejic.202100400

Chemistry Europe
European Chemical Societies Publishing

Nucleophilic Nickel and Palladium Pincer Hydroxides: A Study of Their Reactions with Dimethyl Carbonate and Other Non-Alkylating Organic Electrophiles

Luis M. Martínez-Prieto,[a, b] Diego del Río,[a] Eleuterio Álvarez,[a] Pilar Palma,[a] and Juan Cámpora*[a]

The reactions of the pincer hydroxide complexes [(^{iPr}PCP)M(OH)] (M=Ni, Pd) with dimethyl carbonate (DMC), and a set of organic electrophiles including benzaldehyde have been investigated in the context of our ongoing investigation on the synthesis of alkyl carbonates from CO_2 and alcohols. The final outcome of such reactions is diverse, but for PhCHO and DMC the first step is a mechanistically similar addition of the [M]–OH linkage across the carbonyl functionality, that leads to unstable adducts. DMC is cleaved irreversibly by both Ni and Pd hydroxides, affording the corresponding methylcarbonates [(^{iPr}PCP)MOCO_2Me] and methanol, whereas PhCHO affords benzoate complexes [[(^{iPr}PCP)MOCO_2Ph]. The main kinetic and thermodynamic features of these reactions were reproduced satisfactorily by computational DFT models. The calculations throw light on the true causes of irreversibility of DMC cleavage by nucleophilic hydroxide complexes, which is the primary cause that prevents methanol carboxylation from being catalysed by the Ni or Pd pincers.

Introduction

Pincer ligands and their transition metal complexes offer a privileged platform for the study of the chemical reactivity of complexes that are usually hard to prepare and manipulate.[1,2] Rigid pincers are perfectly adapted to the square planar geometry of Group 10 M(II) ions, to which they confer unusual robustness. For example, hydride complexes[3] with pincer ligands may combine M–H and M–C bonds, and yet they are very stable compounds. On the other hand, the fixed geometry imposed by pincer scaffolds imply that, for square-planar complexes, there is only one possible coordination site available for useful transformations. Though at first glance this might pose a severe restriction, rigid scaffolds like the well-known ^{R}PCP ligands (see Scheme 1 for R = *i*Pr) enhance the chemical reactivity at the vacant site due to the strong *trans* labilizing effect of the central M–C(*pincer*) bond.[4]

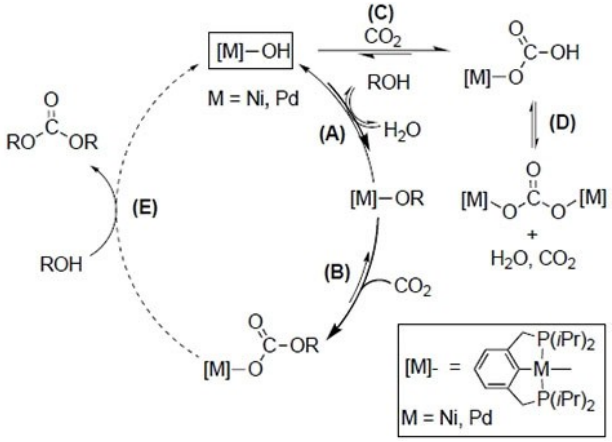

Scheme 1. Hypothetic mechanism for a catalytic alcohol carboxylation process.

It has been known for a long time that strongly basic ligands such as hydroxo, alkoxo or amido become highly reactive in the coordination sphere of late transition metals, due to the lack of suitable empty orbitals to accept π-electron donation from the exceedingly basic electron pairs sitting on the heteroatom.[5] Species containing such reactive M–OH, M–OR or M–NR_2 linkages are key intermediates in various catalytic processes, ranging from commodity industrial processes (like the Wacker reaction)[6] to biocatalysis, e.g. in metalloenzymes like carbonic anhydrase or alcohol deshydrogenase.[7] Furthermore, the nucleophilicity of covalent metal hydroxides played an important role in the historic development Coordination Chemistry.[8] In contrast with the usually well-defined nature of M–C bonds, the chemistry of M–OH or M–OR ensembles is often complicated by their

[a] *Dr. L. M. Martínez-Prieto, Dr. D. del Río, Dr. E. Álvarez, Dr. P. Palma, Prof. J. Cámpora*
Instituto de Investigaciones Químicas,
CSIC-Universidad de Sevilla,
C/Américo Vespucio, 49. 41092, Seville, Spain
E-mail: campora@iiq.csic.es
[b] *Dr. L. M. Martínez-Prieto*
Instituto de Tecnología Química
CSIC-Universidad Politécnica de Valencia,
Avda. de Los Naranjos, s/n. 46022, Valencia, Spain

Supporting information for this article is available on the WWW under https://doi.org/10.1002/ejic.202100400

Part of the "RSEQ-GEQO Prize Winners" Special Collection.

tendency to cancel its basicity forming multinuclear aggregates, to experience irreversible hydrogen elimination processes, or simply by their facile hydrolysis with the slightest moisture traces. Pincer scaffolds offer unique opportunities to overcome these difficulties, opening new avenues to explore the full potential of terminal M-heteroatom linkages, combining classic nucleophilic/basic reactivity patterns with the unique ability of transition metals for the activation of unreactive bonds and small molecules.[9]

One of the long-standing research topics in our group is the analogy between the chemical reactivity of metal-carbon bonds with similar metal-heteroatom bonds in monomeric Ni(II) and Pd(II) complexes with hydroxo, alkoxo or other similar non-dative heteroatom ligands.[10] In our experience, the ^{iPr}PCP scaffold, which contains symmetrical $CH_2P(iPr_2)$ arms, has an adequate balance of steric shielding to promote interesting chemical reactivity while allowing enough stability for isolation purposes. The ^{iPr}PCP pincer has other practical features that facilitate our task, like the stereochemical handle provided by the isopropyl substituents at phosphorus, or convenient monitoring of chemical reactions using the simple single-line $^{31}P\{^1H\}$ NMR spectra of most of their complexes. We found that hydroxide derivatives [(^{iPr}PCP)M(OH)] (M=Ni or Pd) are excellent starting materials, easy to synthesize and handle,[11] and, although the isolation of pure samples of the corresponding alkoxides [(^{iPr}PCP)M(OR)] is challenging,[12,13] their reactions can be readily monitored *in situ*, facilitating the investigation of important processes like β-hydrogen elimination from the alkoxide.[14] Our studies confirmed that hydrolysis of the M–OR bonds is fully reversible. Accordingly, the hydroxides equilibrate with the corresponding alkoxides in the presence of water-alcohol mixtures.[13] Both the hydroxides and alkoxides are efficient nucleophiles. Their reactions with CO_2 bring a typical example and an opportunity for potential applications. These reactions are extremely fast and complete, yielding the corresponding bicarbonates [(^{iPr}PCP)M(OCO_2H)] and alkylcarbonates [(^{iPr}PCP)M(OCO_2R)], respectively. Even though CO_2 insertion is thermodynamically favorable, the products are kinetically labile, leading to partial decarboxylation to binuclear carbonates [{(^{iPr}PCP)M}$_2$(μ-CO_3)], as soon as their solutions are manipulated.[15] However, the same chemical lability of the [M]–OCO_2- linkage enables immediate reversion of the equilibrium mixtures if CO_2 and water or ROH are restored to the system. Furthermore, alkylcarbonates [(^{iPr}PCP)M(OCO_2R)] are thermodynamically favored under equilibrium conditions, in which they are always the prevalent species as long as enough ROH and CO_2 are available, even in the presence of substantial amounts of water. This led us to investigate the possible application of the pincer hydroxides and alkoxides to promote the synthesis of organic carbonates through direct alcohol carboxylation, as shown in Eq. 1 and Scheme 1.[15b,16]

$$2\,ROH + CO_2 \rightleftharpoons CO(OR)_2 + H_2O \quad (1)$$

Alcohol carboxylation has attracted much interest as a potential method for CO_2 fixation and valorization in the form of organic carbonates.[17] Organic carbonates (like dimethyl carbonate, DMC[18]) or polycarbonates are produced in large amounts from toxic or costly intermediates like phosgene or, more recently, epoxides.[17d–e,19] Therefore, direct carboxylation of alcohols has an enormous potential as a "green sink" to capture CO_2 into a variety of valuable chemicals and polymeric materials. Unfortunately, alcohols fail to react spontaneously with CO_2, for both kinetic and thermodynamic reasons.[17a,20] For example, the synthesis of DMC from CO_2 and methanol is exothermic and only slightly endergonic at room temperature. However, in contrast with water, methanol does not react spontaneously with CO_2 to any extent. A number of metal alkoxides, including niobium methoxide or diorganotin methoxides, have been shown to catalyze the carboxylation of methanol, but in general their efficiency is rather low.[17b] After many attempts, we found that pincer Ni and Pd hydroxide or alkoxide complexes fail to promote the synthesis of DMC from methanol and CO_2 under various experimental conditions, ranging from room temperature NMR-tube studies to high pressure and temperature in neat MeOH or supercritical CO_2.[15b,16] Catalytic carboxylation, even as a disfavored equilibrium, was definitively ruled out using isotope labeling experiments. Since processes (**A**) to (**D**), shown in the right side of Scheme 1, were demonstrated to be all facile and fully reversible, it follows that the pitfall that prevents the closing of the catalytic cycle and fixation CO_2 as DMC must lie in the final step (**E**) shown in the left side of the Scheme with a dashed arrow.

To throw some light on the ultimate causes that prevent the catalytic synthesis of DMC as shown in Scheme 1, we decided to investigate the process (**E**) in the reverse direction, namely, studying the cleavage of DMC by nickel and palladium hydroxides. The reactions of organic esters with metal hydroxides and alkoxides are classic subjects of Organic Chemistry.[21] These are involved in such important transformations as ester hydrolysis or transesterification. In recent years, the use of metal alkoxides with well-defined coordination environments has improved the control over some of these reactions, e.g. the ring opening polymerization of cyclic esters.[22] However, in spite of the significance of metal hydroxides in the organic and bio-organic context, studies on the reactivity of well-defined pincer hydroxide complexes have been focused more on the activation of small electrophilic molecules like CO, CO_2 or dihydrogen,[11,15,23–27] than on typical carbonyl electrophiles like ketones, aldehydes or esters. As a part of studies on reduction of carbonyl compounds with pincer hydride species, Guan has reported relevant mechanistic data for some of the above-mentioned reactions,[28] but, as far as we know, no study has been specifically devoted to investigate the interaction of well-defined pincer hydroxides with conventional carbonyl electrophiles. Therefore, to place our work in a broader context, we decided to complete our study on the nucleophilic cleavage of DMC by nickel and palladium pincer hydroxides [(^{iPr}PCP)MOH], by examining their ability to react with some other typical organic electrophiles: benzaldehyde, ketones (acetone, acetophenone) and isocyanides. In addition, we modelled the mechanisms of the reactions with benzaldehyde and DMC by

means of DFT calculations, which we describe in detail in the last part of this contribution.

Results and Discussion

Reactions of nickel and palladium hydroxides [(^{iPr}PCP)M(OH)] with several organic electrophiles

Prior to undertaking our study of the DMC cleavage by pincer Ni and Pd hydroxides [(^{iPr}PCP)M(OH)], we explored their reactions with a few selected electrophiles. The results are summarized in Scheme 2. From this point on, pincer-metal fragments are represented as [M] (with M=Ni or Pd) whenever it is advised for the sake of clarity.

The reactions of the pincer hydroxide complexes with near-stoichiometric amounts of enolizable methylketones are controlled by the weak acidity of the α-methyl group, giving rise to the corresponding enolate complexes. This reaction is well-precedented and there are several reports in the literature describing "neutralization" reactions of basic group 10 organometallic hydroxides with weakly acidic carbonyl compounds.[29,30] Furthermore, it is known that Ni(II) frequently favors the κ-*O* coordination of enolate ligands, whereas Pd leads to κ-C type coordination,[31,32] in line with the lower oxophilicity of the latter.[32b] Accordingly, the reaction of [(^{iPr}PCP)Ni(OH)] with equimolar amounts of acetophenone in C_6D_6 is incomplete and gives rise to equilibrium mixtures of the hydroxide and the corresponding *O*-enolate, unambiguously identified in the solution NMR spectra of the reaction mixtures on the basis of its characteristic ^{1}H and ^{13}C signals of the vinyl enolate fragment. The apparent equilibrium constant, $K_{eq} \approx 2 \times 10^{-2}$, is very similar to that measured for the analogous reaction of acetophenone with the monomeric hydroxide complex [Ni(Me)(OH)(dippe)].[29a] Removing water with molecular sieves shifts the equilibrium to the enolate side until the hydroxide/enolate ratio reaches 3:7, but the *O*-enolate product was reluctant to crystallize and could not be isolated pure (see Experimental Section). In contrast, [(^{iPr}PCP)Pd(OH)] reacts clean and irreversibly with acetone, giving rise to the corresponding *C*-enolate (or ketonyl[32]) complex [(^{iPr}PCP)Pd(CH_2COCH_3)], which was readily isolated as a stable white solid.[30]

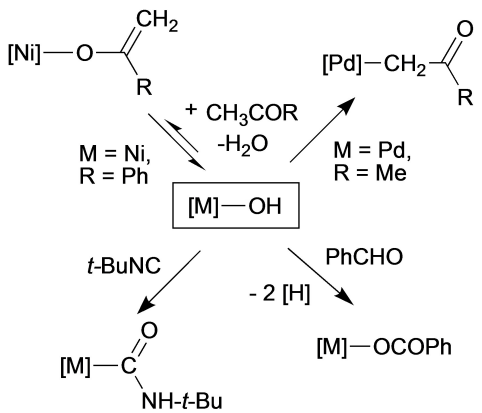

Scheme 2. Reactions of the Ni and Pd pincer hydroxides with carbonyl-based electrophiles and isocyanides (here, [M] represents the pincer fragment [(^{iPr}PCP)M)] with M=Ni or Pd, except where the metal is specified).

The Pd hydroxide reacts in THF solution with benzaldehyde which, lacking acidic hydrogens, can only undergo nucleophilic attack at the carbonyl functionality. ^{31}P NMR monitoring reveals the formation of a main product characterized by a singlet resonance at 60.4 ppm. Full conversion requires an excess of reagent (up to 3:1 ratio). A sample of the main product, contaminated with a small amount of PhCHO, was isolated after solvent evaporation under vacuum (see experimental) which led to its identification as the benzoate [(^{iPr}PCP)PdOCOPh]. The nickel hydroxide behaves similarly but the reaction with PhCHO is sluggish, requiring using neat PhCHO (reagent ratio ≈100:1) to complete the transformation within a reasonable time frame. However, the ^{31}P{^{1}H} NMR spectrum of the reaction mixture suggests that the reaction proceeds cleanly to yield a single product (singlet at δ 57.7 ppm). In order to confirm the identity of the Ni and Pd benzoate complexes, their spectral properties were compared with those of authentic samples, independently synthesized by reacting equimolar amounts of the corresponding hydroxides with benzoic acid. For the sake of completeness, the reactions of the more reactive palladium hydroxide with *p*-nitrobenzaldehyde and *p*-dimethylaminobenzaldehyde were carried out in NMR tubes, and the corresponding *p*-substituted benzoate complexes were prepared to confirm the identity of the products (see below).

In a previous contribution, we have shown[11] that the reaction of Ni and Pd hydroxides [(^{iPr}PCP)M(OH)] with CO leads to unstable hydroxycarbonyl complexes, [M]–COOH. These evolve in solution, undergoing partial decarbonylation to yield isolable CO_2-bridged species [M]–COO–[M].The mechanism of CO insertion into Ni–OH bonds has attracted much interest because it is involved in some catalytic processes and has also relevance in biological methanogenesis.[10] Further examples of carbonylation of Ni or Pd pincer hydroxide complexes were reported later.[23a,27] As in the case of CO_2 (see Scheme 1), the formation of [M]–COO–[M] from [M]–COOH implies some degree of reversibility of CO insertion. DFT calculations suggest a migratory-type insertion mechanism (*i.e.*, CO interacts first with the metal, and then the hydroxide "migrates" to the carbonyl C), albeit assisted by the nonbonding electron pairs localized on the hydroxyl O atom.[33] Thus, it is intriguing that the formally analogous reactions of well-defined hydroxide complexes with isocyanides (which are isoelectronic with CO), remain almost unknown.[34]

To complete this study, we briefly examined the reaction of [(^{iPr}PCP)M(OH)] hydroxides with *t*-BuNC. The reaction is fast and selective in both cases, yielding stable products that were isolated as yellow (M=Ni) or white (M=Pd) powdery solids, as shown in Scheme 2. The presence of a carbamoyl functionality (*i.e.*, [M]–C(=O)NH*t*-Bu), was deduced from their IR and solution NMR spectra. Strong IR absorptions at 1550 cm^{-1} and a low field ^{13}C resonances (at 210 and 205 ppm for Ni and Pd, respectively, with characteristic triplet splitting by coupling with two equivalent ^{31}P nuclei) demonstrate the presence of a –C(=E)E'H fragment (E and E' could be either O or N-*t*Bu), carbon-

connected to the metal. In both products, the ^{1}H signal corresponding to the NH was located in the proximity of 5.0 ppm. That the hydroxyl hydrogen atom migrates to the more basic nitrogen was deduced from the observation of NOE cross-peaks that correlate the latter signals with that of the *t*-Bu group (a singlet at *ca.* 1.5 ppm) in the 2D NOESY spectra of both products. Similar Pd and Pt carbamoyl complexes have been synthesized in a more straightforward manner by carbonylation of amido complexes.[35]

Among the electrophiles whose reactions with the Ni and Pd hydroxides have been presented in this section, PhCHO is the one that bears a closer resemblance to organic carbonates. This is also a classic substrate for the investigation of nucleophilic attack on organic carbonyl functionalities. Thus, we examined more closely this reaction, focusing on the more reactive palladium hydroxide. The formation of the benzoate product [(^{iPr}PCP)PdOC(O)Ph] from [(^{iPr}PCP)PdOH] and PhCHO implies the formal loss of two hydrogen atoms. These could be either taken up by some hydrogen acceptor, or released free as H_2 (Equation 2 and Equation 3).

$$[M]\text{-}OH + 2\ PhCHO \longrightarrow [M]\text{-}OCOPh + PhCH_2OH \quad (2)$$

$$[M]\text{-}OH + PhCHO \longrightarrow [M]\text{-}OCOPh + H_2 \quad (3)$$

Eq. 2 is directly related to the well-known Cannizaro reaction, whereby non-enolizable aldehydes react with aqueous alkali hydroxides to afford 1:1 mixtures of carboxylate and alcohol. In this reaction, the hydrogen acceptor is a second equivalent of the aldehyde, which ends up as benzyl alcohol. Indeed, GC analysis of the crude reaction mixtures of the Pd hydroxide with PhCHO reveals the presence of benzyl alcohol, but the amount is far too small to account for the equimolar ratio expected according to Eq. 2. This suggests that most of the remaining hydrogen could be escaping from the system as H_2, as shown in Eq. 3. Figure 1 shows the course of the reaction of [(^{iPr}PCP)PdOH] (0.05 M in THF) with 3 equiv. of PhCHO at 25 °C, simultaneously monitored by GC and $^{31}P\{^{1}H\}$ NMR over a period of 24 h. The last measurement showed that about 90% of the starting hydroxide had been consumed, and 75% of the total ^{31}P intensity corresponded to the signal of the benzoate complex. In contrast, benzyl alcohol (determined by GC) amounted to just 17% with regard to the starting hydroxide. In addition to the ^{31}P resonances of the starting material [(^{iPr}PCP)Pd(OH)] and the product [(^{iPr}PCP)Pd(OCOPh)] (at *ca.* 59 and 61 ppm, respectively), only a low-intensity signal was observed at 71.7 ppm, whose chemical shift coincides with the characteristic low field-shifted signal of the pincer hydride [(^{iPr}PCP)PdH].[36]

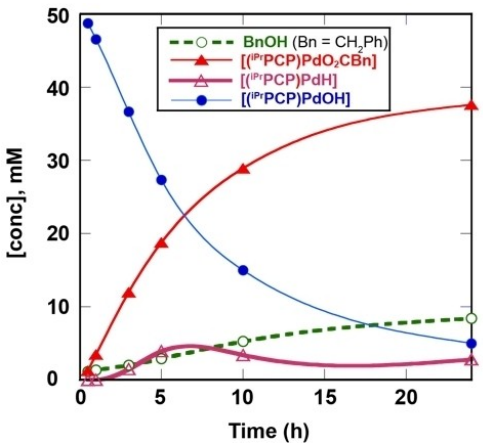

Figure 1. Concentration profiles of the key species involved in the reaction of [(^{iPr}PCP)PdOH] (0.05 M in THF) and PhCHO (3-fold excess) at room temperature, as determined using ^{31}P NMR and GC.

The formation of detectable amounts of the Pd hydride complex is mechanistically significant. In contrast with the hydroxide and the benzoate complexes, which exhibit monotonous decay and rising trends, respectively, the concentration of the hydride reaches a maximum after 5 h (8%) and then stays quasi-stationary, decaying very slowly as the reaction advances towards completion in the following hours. This behavior suggests that the hydride complex is a reaction intermediate. From the fact that the hydride ligand can only originate from the aldehyde functionality, we deduce that the attack of the palladium hydroxide leads to an unstable insertion complex, most likely a classic "tetrahedral intermediate",[37] [Pd–OC(H)(Ph)(OH)], which then decomposes by β-H elimination, as proposed in Scheme 3. We have demonstrated previously that, despite the strong stabilizing effect of PCP pincer ligands, Ni and Pd methoxides [(^{iPr}PCP)M(OMe)] undergo reversible β-H elimination above the room temperature, affording detectable amounts of the corresponding hydride, which slowly decomposes to afford M(0) species.[14]

As shown also in Scheme 3, two parallel processes compete in trapping the palladium hydride. The main one is the direct reaction of the hydride with benzoic acid formed in the β-elimination step. This route leads directly to the final benzoate complex, plus H_2, *i.e.*, it is responsible for the acceptorless stoichiometry described in Eq. 3. In line with this hypotheses, the NMR spectra of mixtures of [(^{iPr}PCP)Pd(OH)] with substituted aldehydes *p*-ZC_6H_4CHO (Z=NMe_2 or NO_2) showed visible differences in the intensity of the characteristic ^{31}P signal of the hydride intermediate, that correlate with the strength of the

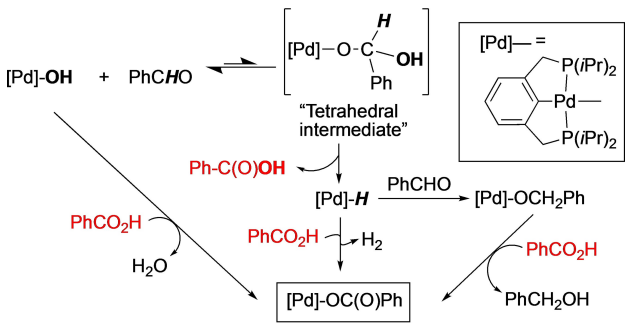

Scheme 3. Proposed mechanism for the reaction of [(^{iPr}PCP)Pd(OH)] with PhCHO.

corresponding carboxylic acid. For Z=NMe$_2$ the weakness of the acid allowed the buildup of higher concentrations of the hydride, whereas with Z=NO$_2$, its ^{31}P signal was so weak that is hardly detectable. The benzyl alcohol detected by GC in the Pd reaction, characteristic of the Cannizaro-type stoichiometry (eq. 2), originates in the second pathway, that involves the capture of [Pd]–H by benzaldehyde, followed by reaction of the resulting benzoxide with benzoic acid. Similar aldehyde hydrometallations play an important role in reactions catalyzed by pincer-stabilized hydrides.[28] Since the ^{31}P signal for the resulting benzoxide intermediate [(^{iPr}PCP)Pd(OCH$_2$Ph)] was not observed (this compound is still unreported, but its ^{31}P signal is expected to occur within a region 2–4 ppm upfield of the signal of the starting hydroxide[13j]), it can be assumed that the subsequent neutralization of the benzoxide and benzoic acid outcompetes the hydrometallation reaction. In addition, the persistence of some [(^{iPr}PCP)Pd(H)] at the end of the reaction suggests that some of the benzoic acid formed in the main process could be trapped also by the starting hydroxide, as suggested in Scheme 3.

Direct evidence for this mechanism was provided by the identification of the unstable tetrahedral intermediate in the NMR spectra of mixtures of [(^{iPr}PCP)Pd(OH)] and PhCHO at subambient temperature (see SI). When the ^{31}P{^{1}H} spectrum of a freshly prepared 0.1 M solution of the palladium hydroxide and PhCHO (1:1) in toluene-d_8, was recorded at −30 °C, it showed an additional resonance at 56.1 ppm that was not observed at room temperature. The new signal, with intensity 1/2.3 of that of the starting hydroxide, is only 0.6 ppm apart from the latter. The spectrum is quite clean since, other than these two resonances, only the incipient signals of the hydride and benzoate complexes were detected, at 71.7 and 60.3 ppm, respectively. The −30 °C ^{1}H NMR spectrum (Figure S1) confirmed that the major P-containing species is still the hydroxide, unambiguously revealed by its characteristic high-field OH signal at −1.23 ppm. Two small resonances corresponding to a partially resolved AX spin system were observed in an otherwise clean region, at 6.36 (sharp doublet, $^3J_{HH}$ = 7.5 Hz) and 5.35 ppm (broad). These are assigned to the methyne and OH protons, respectively, of the hemiacetal functionality (–OCH(O*H*)–) of the hydroxide-benzaldehyde adduct. This phenomenon is reversible and the signals of the labile adduct disappeared when the spectrum was recorded again at room temperature. Repeating the experiment with a three-fold excess of PhCHO causes the signals of the adduct to become of comparable intensity to those of the hydroxide complex, which enabled us to gather some key ^{13}C data. For example, the ^{13}C resonance corresponding to the hemiacetal methyne was located at 96.3 ppm in the 2D ^{1}H-^{13}C HSQC spectrum. The $^1J_{CH}$ coupling (153 Hz) is compatible with a hemiacetal-type sp^3 carbon. As expected, both ^{1}H resonances at 6.36 and 5.35 ppm were further broadened by chemical exchange. The 2D phase-sensitive NOESY/EXSY spectrum (Figure S2) shows that each signal of free PhCHO is connected to another one in the adduct through exchange crosspeaks. Most evident is the characteristic aldehyde signal at 9.57 ppm with the acetal methyne at 6.36 ppm. In addition, the assignment of the broad 5.35 ppm signal to the hemiacetal hydroxyl was confirmed by an exchange crosspeak with a minor signal at 4.45 ppm, due to a small amount of water in the sample. These data conclusively demonstrate that the [(^{iPr}PCP)Pd(OH)]/PhCHO mixture is in equilibrium with a labile addition product with hemiacetal structure. The relative intensities of the ^{31}P resonances in the low temperature spectra allow an estimation of $K_{eq} \approx 5$ at −30 °C, corresponding to a slightly negative $\Delta G°$ (*ca.* −0.7 Kcal·mol^{-1} at 243 K).

Cleavage of DMC by Ni and Pd Pincer Hydroxides

As mentioned in the introduction, our previous studies on the pincer alkoxide/CO$_2$/MeOH system have shown that the pitfall of the catalytic process shown in Scheme 1 is within step (**E**). Admitting that this is a mechanistically simple process, the microscopic reversibility principle dictates that its reversal, namely, cleavage of DMC by the Ni and Pd pincer hydroxides should proceed through the same but inverse mechanistic sequence. In consequence, any thermodynamic or kinetic rate measurement pertaining to the process depicted by Eq. 4 would be also relevant to process (**E**). In an effort to unveil the causes, we decided to investigate the reactions of hydroxides [(^{iPr}PCP)M(OH] whether the process shown Eq. 4 does in fact occur.

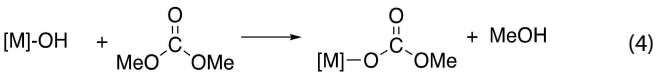

(4)

Preliminary experiments in C$_6$D$_6$ solution showed that both pincer hydroxides do react very slowly with DMC, though appreciably faster with the Pd complex. Somewhat disappointingly, NMR analyses of the reaction mixtures revealed the formation of the expected alkylcarbonate [(^{iPr}PCP)Pd(OCOOMe)] admixed with binuclear carbonate [{(^{iPr}PCP)Pd}$_2$(μ-CO$_3$)] and unreacted hydroxide, whereas for M=Ni, most of the starting material hydroxide remained, and only a small amount of the corresponding carbonate [{(^{iPr}PCP)Ni}$_2$(μ-CO$_3$)] was formed. Therefore, we decided to run both reactions in neat DMC, using ^{31}P{^{1}H} NMR to monitor the advance of the reaction. To avoid ambiguous assignments, the spectra were referenced with regard to external PPh$_3$ in C$_6$D$_6$ (see the Experimental Section for details). Using gas-tight PTFE-valve sample tubes, both reactions proceed in a well-behaved manner, with no significant decay of the pincer framework over long reaction times. As anticipated by the preliminary experiments, the course of these reactions appear more complicated than suggested by Eq. 4. The reason is the lability of the [M]–OCOOR linkage, which allows facile exchange of the OR unit, as previously reported.[15b] This is shown in Figure 2, which displays the ^{31}P{^{1}H} NMR monitoring of the reaction of [(^{iPr}PCP)Ni(OH)] with DMC at 50 °C (left) and 80 °C (right). These experiments allow distinguishing two distinct stages in the reaction. The behavior of the Pd hydroxide is essentially the same, except that the reaction proceeds faster and the stages were not so clearly differentiated (see below). For convenience, the following discussion will focus

Full Papers
doi.org/10.1002/ejic.202100400

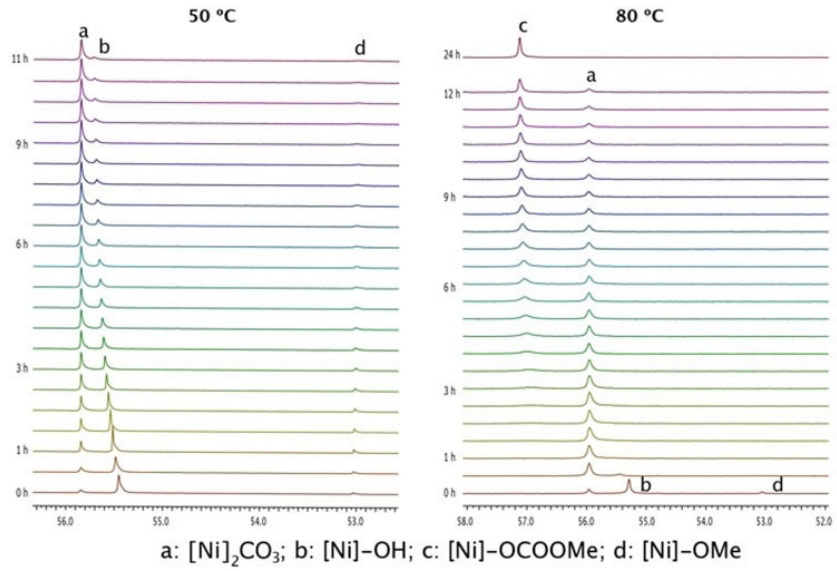

Figure 2. $^{31}P\{^{1}H\}$ spectra of a solution containing 25 μmol of [Ni]OH in neat DMC at two different temperatures: 50 °C (left) and 80 °C (right). ([Ni] stands for the [(^{iPr}PCP)Ni] fragment).

on the reaction with the nickel complex, but the same conclusions can be applied to the Pd system.

As can be seen in the left side of Figure 2, the reaction appears to be almost complete after 11 h at 50 °C, since very little hydroxide (signal tagged **b**) remains in the sample at this time. The signal of the main product, **a**, occurs at 55.9 ppm, which matches that of the binuclear carbonate [{(^{iPr}PCP)Ni}$_2$(μ-CO_3)], as observed in the previous experiments. This was confirmed by comparison with an authentic sample[15a] of the carbonate recorded in the same conditions. This suggests that the reaction involves *double* cleavage of DMC, according to the stoichiometry shown in Eq. 5.

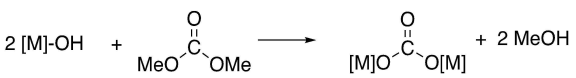

(5)

In addition to signal **a**, a low intensity signal, **d**, was observed at 53.0 ppm. The chemical shift for this resonance is distinct enough from those of **a** and **b**, allowing its assignment to the methoxide complex, [(^{iPr}PCP)Ni(OMe)] (52.6 ppm in C_6D_6).[11] The latter can arise by methanol/water exchange with the remaining hydroxide complex, as shown in Eq. 6, see below.[13] Accordingly, signal **d** grows broader as the exchange rate is accelerated by the water and methanol, and ultimately fades in the baseline when the hydroxide complex is nearly depleted by its reaction with DMC in the last few spectra shown on the top. Another effect of the rising concentration of methanol and water is the visible drift of the [(^{iPr}PCP)Ni(OH)] signal, **b**. The position of this signal "senses" the concentration of acidic molecules because the basic hydroxide ligand is a powerful hydrogen bond acceptor. To verify this effect, we conducted an NMR titration of a 0.037 M solution of [Ni]–OH with water in C_6D_6 at room temperature, using both the ^{31}P and ^{1}H channels (see SI, Figures S3 and S4). We observed an approximately linear dependency of the chemical shift of the ^{31}P resonance on the amount of added water, from 55.2 ppm in anhydrous benzene to 56.0 ppm in the presence of 3 mole-equivalents of water. The magnitude and sign of this effect resembles the one observed in Figure 2. The hydroxyl ^{1}H resonance retained its characteristic triplet structure (due to coupling to ^{31}P) until the NiOH/H_2O ratio reached 1 : 1, indicating that chemical exchange between the coordinated hydroxide ligand and free water is slow on the NMR timescale. The capacity of hydroxide complexes to accept strong hydrogen bonds is supported by the formation of isolable hydrates. The [(^{iPr}PCP)Pd(OH)] was shown to crystallize as a binuclear hydrate containing a doubly hydrogen-bridged water molecule linking the OH ligands of each moiety.[11] We now report the X-ray diffraction structure of its nickel analogue (see SI). Crystals of this well-defined hemihydrate were reproducibly grown from concentrated solutions of [(^{iPr}PCP)Ni(OH)] in moist diethyl ether. The O···O distances (2.819(4) Å) are significantly longer than in its Pd analogue (2.768(11) Å, avg.),[11] implying that H bond is stronger in the latter.

Whereas the above observations apparently contradict the straightforward result anticipated in Eq. 4, we realized that longer reaction times cause the appearance of a new signal (**c**) at 56.8 ppm, which corresponds to the expected alkylcarbonate, [(^{iPr}PCP)Ni(OCO_2Me)] (56.5 ppm in C_6D_6).[15b] As can be seen in the right side of Figure 2, signal **c** rapidly becomes prevalent when the reaction is carried out at 80 °C. At this temperature, the conversion of the starting hydroxide complex into the binuclear carbonate takes just a few minutes (see spectra at the bottom of the right figure). From that point on, the signal of the carbonate complex (**a**) is gradually replaced by that of the methylcarbonate (**c**). Note that the methoxide (signal **b**), visible in the initial stages of the experiment, rapidly disappears, too. In conclusion, at 80 °C the reaction is clean and complete within

24 h (top spectrum), the whole process being as expected according to Eq. 4. As mentioned above, the reaction of the Pd hydroxide in neat DMC proceeds much more readily than for Ni. The signal of the [(^{iPr}PCP)PdOCO$_2$Me] becomes noticeable shortly after mixing at room temperature, and the transformation is complete after 24 h at 50 °C. Figure 3 shows the evolution of the ^{31}P-containing species plotted against time in the Ni and Pd systems, at 50 and 25 °C, respectively.

The apparent complexity of the reactions of the hydroxides with DMC could have been foreseen on the basis of our previous investigations, summarized in Scheme 1. The binuclear carbonate and methoxide complexes arise as a consequence of rapid exchange equilibria which, within the range of temperature explored, are much faster than the cleavage of DMC. The whole process can be represented by a simple three-equation set: 4b, 6 and 7. We have shown before that the equilibria shown in Eq 7 are strongly temperature-dependent.[15] At room temperature (M=Pd) or above (M=Ni), these are shifted to the right side, reducing the amount of hydroxide complex available to react with DMC. This nearly stops the latter reaction. Increasing the temperature to 80 °C allows overriding equilibrium 7, which gradually reverts, giving back the hydroxide complex sequestered in the binuclear carbonate. Eventually, the whole ^{31}P intensity ends up in the single, intense peak **c** (Figure 2, right side). At this point, the overall stoichiometry of the process matches Eq. 4.

Despite the complexity of the kinetic system, our results could be reasonably well modeled on the basis of equations 9b, 11 and 12, using numerical kinetic simulation software.[38] Our kinetic model describes the initial step as irreversible, and explicitly includes the forward and backward steps for Eqs. 11 and 12. The small deviation observed in the fitting of the palladium plot could be attributed to the difficult integration of the broad ^{31}P resonances of the hydroxide and methoxide signals, which are lost at an early stage of the experiment. This simple model also avoids explicit consideration of bicarbonate complexes, ([(^{iPr}PCP)M(OCO$_2$H)], which should be part of the equilibrium (see Scheme 1), but were not detected. Independently of the metal, the concentration of the bicarbonate complex is expected to be fairly small. Fast exchange also contributes to the loss of these signals. Notwithstanding these shortcomings, the simplified model accounts for all the main features of the plots and provides reasonably good thermodynamic and kinetic data to be used as benchmarks for DFT calculations.

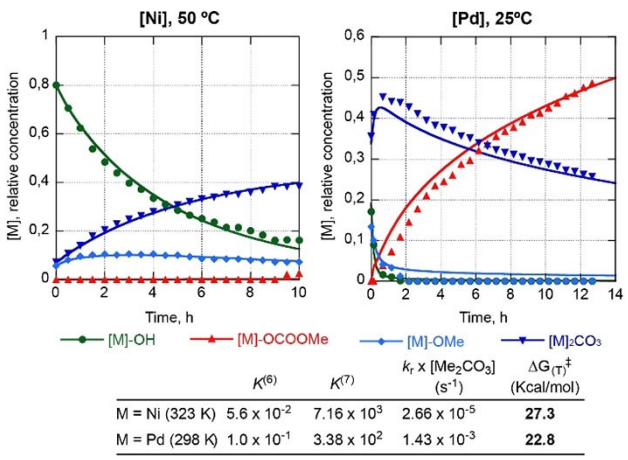

	$K^{(6)}$	$K^{(7)}$	k_r x [Me_2CO_3] (s^{-1})	$\Delta G_{(T)}^{\ddagger}$ (Kcal/mol)
M = Ni (323 K)	5.6 x 10^{-2}	7.16 x 10^{3}	2.66 x 10^{-5}	**27.3**
M = Pd (298 K)	1.0 x 10^{-1}	3.38 x 10^{2}	1.43 x 10^{-3}	**22.8**

Figure 3. Evolution of the ^{31}P-containing species involved in the reaction of hydroxides [M]–OH with DMC at 50 °C (M=Ni) and 25 °C (M=Pd). Solid lines represent numerical fitting of the experimental data to the kinetic model represented by eqs 4b, 6 and 7.

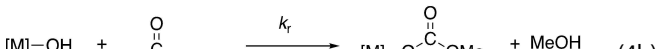

(4b)

(6)

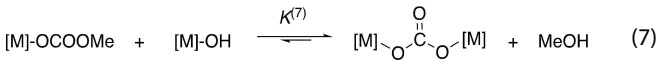

(7)

DFT analysis of the nucleophilic reactions of Ni and Pd pincer hydroxides with PhCHO and DME

In a previous work,[13] we showed that the GGA functional PBE, in combination with an implicit solvent model (CPCM), satisfactorily reproduces the experimental geometry and key vibrational frequencies of ^{iPr}PCP alkoxide complexes of Ni and Pd, at a low computational cost. Other authors concur in that PBE produces accurate geometries for transition metal complexes and is also good for approximate thermochemical data.[39] In this work, we have applied some additional refinements to the above methodology, which improve the quality of the results without increasing significantly their computational cost (see Computational Details in the Experimental Section).

Even for a few relatively simple reactions, predicting the preferred configuration of the pincer *i*Pr substituents in each intermediate, although feasible, increases very significantly the computational effort. Therefore, we removed conformational uncertainty by replacing *i*-propyl substituents by methyl groups (*i.e.*,^{Me}PCP ligand instead of ^{iPr}PCP). In our own experience,[14b,15a] and also for others,[26,28b] this simplification does not have excessive impact on the main conclusions. As shown below, the agreement between experimental and computed data proves satisfactory in general.

Since the focus of this work is on the nucleophilic reactivity of the Ni and Pd complexes [(^{ipr}PCP)M(OH)], we limited our analysis to the attack of the hydroxides on the carbonyl functionality of PhCHO and DMC and the release of the primary products (benzoic acid and methanol, respectively), leaving aside the non-essential equilibria that complicate both systems. Scheme 4 and 5 display the models used in each calculation, and their results are summarized in the corresponding free energy profiles (Figure 4, Figure 5 and Figure 6). Relative values of free (ΔG) and ZPE-corrected electronic energies (ΔE; ZPE = Zero-Point Energy correction, in italics) are explicitly shown

Full Papers
doi.org/10.1002/ejic.202100400

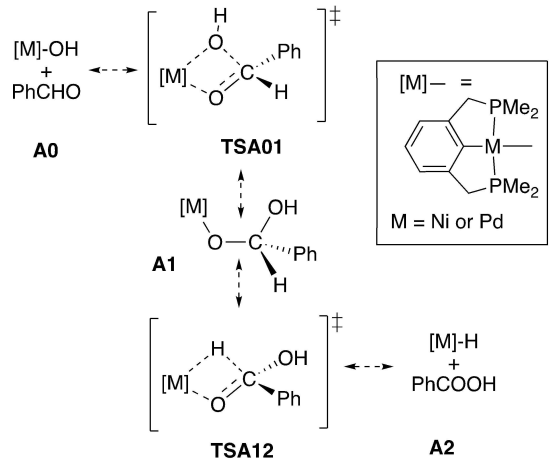

Scheme 4. Simplified mechanism of the reaction of Ni and Pd pincer hydroxides [(^{Me}PCP)M(OH)] with benzaldehyde, as used in DFT calculations.

next to each mark in the profiles. Full details including the breakdown of the different contributions to the energy values and atomic coordinates for each individual molecule can be found in the SI.

Scheme 4 describes the initial stages of the reactions of the Ni and Pd hydroxides [(^{Me}PCP)M(OH)] with benzaldehyde, to afford equimolar mixtures of the corresponding hydride [(^{Me}PCP)M(H)] and benzoic acid. The sequence begins with the starting materials (jointly termed **A0**), namely, the hydroxide complex and benzaldehyde, and concludes at **A2**, an equimolar mixture of benzoic acid and the corresponding hydride complex. The energies of **A0** and **A2** are the sum of its individual components, *i.e.*, two non-interacting molecules. **A0** is conventionally taken as the origin ("zero") of energies in each of the mechanistic pathways (M=Ni or Pd). On the whole, these are simple mechanisms involving a single intermediate, the "tetrahedral" adducts, **A1** (M=Ni or Pd). These are connected to **A0** and **A2** through the corresponding transition states (TS), **TSA01** and **TSA12**. To locate these transition states, we started from the optimized geometries of **A1**, imposing progressively shorter distances between the metal center to either the hydroxyl O atom (for **TSA01**), or to the acetal H atom (for **TSA12**). Intrinsic Reaction Coordinate (IRC) calculations on the optimized TS geometries confirmed that: i) the transition states do correspond to the intended processes; and ii) there are no additional stationary points along the reaction pathway. Both **TSA01** and **TSA12** can be seen as intramolecular σ-bond concerted exchanges whereby the [M]–OC bond of **A1** is displaced by the vicinal hydroxyl or hydrogen, leading to new [M]–OH (in **A0**) or [M]–H (in **A2**), respectively.

As can be seen in Figure 4 (solid lines), the reactions of the Ni and Pd hydroxides with benzaldehyde in THF at 298 K show similar profiles. In either case, formation of the **A1** adduct from **A0** is endergonic, slightly more so for Ni ($\Delta G^{o} = +$ 5.5 Kcal·mol^{-1}) than Pd (+3.4). The moderate energy barriers of less than 20 Kcal·mol^{-1} imply that the initial attacks on the carbonyl are effectively reversible processes. The next step, β-hydrogen elimination, is exergonic and affords benzoic acid and hydride complex (Ni, −3.3; Pd, −7.7 Kcal·mol^{-1}). The energy barriers for β-elimination (**TSA12**) are 4–5 Kcal·mol^{-1} higher than for the nucleophilic attack (**TSA01**). In consequence, the energy of **TSA12** (β-H elimination from **A1**), poses the main

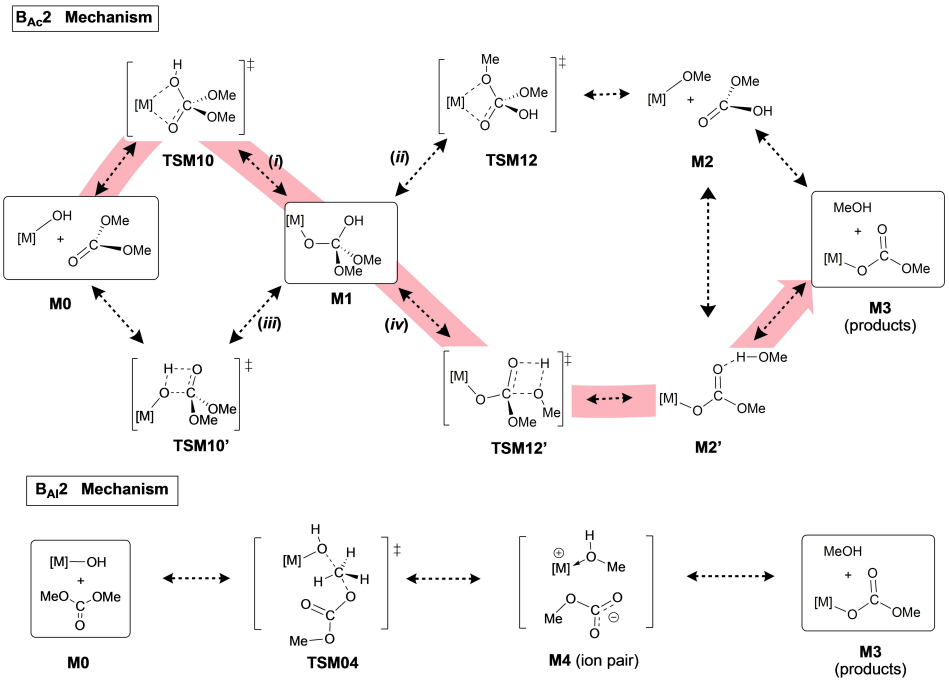

Scheme 5. Computational model used to explore different mechanistic pathways for the reaction of nickel and palladium hydroxide pincer complexes with DMC. The least energy pathway is highlighted.

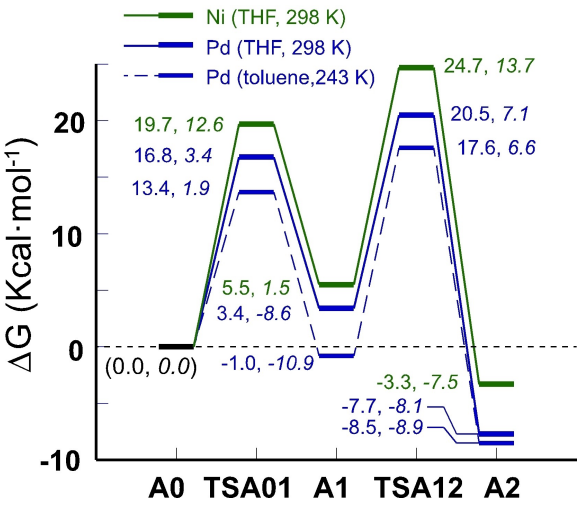

Figure 4. Free energy profile (PBE(CPCM)/6-31G*//PBED3(CPCM)/6-311 + + G(3df,2p)) for the attack of Ni and Pd pincer hydroxides [(^{Me}PCP)MOH] to benzaldehyde. Solid lines represent the profiles for Ni (green) and Pd (blue) in THF at room temperature. The dashed line plot represents the same mechanism for M=Pd in toluene at low temperature (223 K), to match the available experimental data. Explicit figures (Kcal·mol^{-1}) for the free energy (ΔG plain fonts) and ZPE-corrected electronic energies ($\Delta(E(SCF)+ZPE)$, in italics) are shown next to each point in the calculation. Within each calculation series, data are relative to **A0** (the sum of contributions from independent molecules of benzaldehyde and the Ni or Pd hydroxide complex).

energy barrier or, in other words, β-H elimination is the rate determining step. The barriers are not too high, either for Ni or Pd ($\Delta G^{\ddagger}$(**TSA12**)-$\Delta G°$(**A1**) ≈ 19.2 and 17.1 Kcal·mol^{-1}, respectively), but for both metals, **TSA12** lies *ca.* 28 Kcal·mol^{-1} high, which is just enough to render reversibility unlikely at the ambient temperature. This means that, in line with the experimental observations, formation of the adduct **A1** from **A0** can be regarded as a reversible equilibrium preceding the irreversible, rate-determining β-H elimination process. For a better comparison with the experiment, Figure 4 shows the free energy profile for palladium in toluene at T = 243 K (−30 °C). Recall that it was under those conditions that a "tetrahedral intermediate" (analogous to **A1-Pd)** was experimentally detected in solution. Accordingly, the calculation shows that the thermodynamic balance for intermediate **A1-Pd** improves at this temperature becoming slightly exergonic, with $\Delta G° = -1.0$ Kcal·mol^{-1}, which, considering the simplifications in the computational model, compares very well with the experimental value, −0.7 Kcal/mol^{-1}, deduced from low temperature NMR data.

The energy barriers for the **A0**→**A1** step, given by **TSA01**, may be regarded as a gauge for the relative nucleophilicity of the Ni and Pd hydroxides. In both cases, the $\Delta G^{\ddagger}$ associated to **TSA01** are low enough to render the process accessible at room temperature (< 20 Kcal·mol^{-1}), hence both hydroxide complexes are competent nucleophiles. However, for Pd the barrier is 2.9 Kcal·mol^{-1} lower than for Ni ($\Delta\Delta G^{\ddagger}_{(Ni\text{-}Pd)} = 19.7–16.8$, see Figure 4), implying that the palladium hydroxide is a significantly stronger nucleophile than its nickel analogue. The palladium adduct **A1** is also more stable by 1.9 Kcal/mol ($\Delta\Delta G°_{(Ni\text{-}Pd)}$). Note, however, that the Gibbs energies of **TSA01** and **A1** relative to **A0** contain strong thermal contributions that arise from the negative entropy associated to bimolecular processes. ZPE-corrected energies, ΔE, being a temperature-independent parameter, are useful to calibrate the intrinsic reactivity of both hydroxides. As can be seen, although the numerical value of the ΔE-based barriers are smaller than those from ΔG, the ΔE profiles of Ni and Pd show even sharper differences. For **TSA01**, the differential energy barrier, $\Delta\Delta E^{\ddagger}_{(Ni\text{-}Pd)}$, is 9.2 Kcal·mol^{-1}. The same happens with difference of relative energies of **A1-Ni** and **A1Pd** ($\Delta\Delta E_{(Ni\text{-}Pd)} =$ 10.1 Kcal·mol^{-1}), which suggest a much more exothermic process for Pd. Therefore, the thermal (entropy) effect is actually levelling, rather than enhancing the reactivity difference between the Ni and Pd hydroxides. The lower reactivity of the Ni hydroxide suggests that the [Ni]–OH bond might be harder to break than the [Pd]–OH. Indeed, in our own estimation[13] for the (^{iPr}PCP)M pincer system, the [Ni]–OH bond is stronger than the [Pd]–OH bond by *ca.* 4.5 Kcal mol^{-1}. The difference is mainly due to the stronger attractive electrostatic contribution for the smaller-sized Ni(II) cation. However, this quantity alone is still insufficient to explain the large differences in $\Delta\Delta E^{\ddagger}_{(Ni\text{-}Pd)}$. A different but related cause would be steric effects. In line with this interpretation, the ZPE correction is the main contributor to the large $\Delta\Delta E^{\ddagger}_{(Ni\text{-}Pd)}$ figure (see SI, Table S4), which is probably due to the restriction of some normal vibration modes in the more encumbered coordination environment in the smaller Ni(II) atom. In consequence, it can be concluded that the different nucleophilicity of the Ni and Pd hydroxides towards PhCHO stems from the smaller radius of the Ni(II) atom, which is exerted at two different levels, namely, by increasing the strength of the [M]–OH bond, and by relaxing the steric crowding in the larger Pd center.

In modeling the reactions of the pincer hydroxides with DMC, we had to consider at least two main mechanisms that are known to occur in the reactions of organic esters with nucleophiles (Scheme 5).[21] The most frequent one, termed $B_{Ac}2$, leads to the scission of the acyl-oxygen bond (RC(O)–OC), while the so-called $B_{Al}2$ mechanism cleaves the ester bond (RC(O)O–C). The latter can be regarded a particular case of the S_N2 mechanism in which the carboxylate group plays the part of the leaving group. The $B_{Al}2$ mechanism is less frequent than the $B_{Ac}2$, but usually occurs when the ester C–O bond is "activated" by an electron-withdrawing or electrophilic acyl moiety. DMC is a good example of this duality because, depending on the type of nucleophile and the experimental conditions, it may favor typical ester reactivity, undergoing classic $B_{Ac}2$ reactions or it may act as a mild methylating reagent through the $B_{Al}2$ mechanism.[18]

The $B_{Ac}2$ pathway resembles the above-discussed mechanism for the reactions with benzaldehyde, in the initial nucleophilic attack on the ester carbonyl, which gives rise to a similar "tetrahedral intermediate", **M1**. Therefore, to search for the different pathways that connect this intermediate with the starting materials (**M0**) to the products (**M3**), we applied a similar strategy, and systematically explored intramolecular

exchange processes within **M1**. Thus, pathway from **M1** to **M0** was found by forcing the approach of the carbon-bound OH to the metal center (step *i* in Scheme 5). After optimizing the TS geometry highest energy points, the corresponding transition states **TSM10** were located for both M=Ni and Pd. A similar operation, driving the approach of one of the C-bound methoxy groups to the metal center, leads to **TSM12**, which describes a concerted intramolecular σ-bond exchange route to **M2** (step *ii*). Another analogy with the reaction with PhCHO mechanism can be found in the reactive nature of the **M2** couple, formed by the strongly basic methoxides [M]–OMe and the monomethyl ester of carbonic acid, which should be regarded as a kind of carboxylic acid. Mutual neutralization of both partners to yield the final products **M3** is expected to occur very readily. A mechanism composed by processes, *i* and *ii* is appealing because one of the experimentally detected intermediates, the methoxides [M]–OMe, emerges naturally from the reaction sequence. Recall, however, that the kinetic model shown in Figure 3 assumes that the methoxide is formed in a fast side equilibrium, therefore process *ii* is not required to fit the experimental facts. Furthermore, although monomethyl carbonate has been shown to be stable in solution over short periods in rigorously anhydrous solution, this is an unstable molecule that readily decomposes in the presence of water.[40] Therefore, we sought alternative decomposition processes for **M1**. The key feature of **M1** is the M–OC(OH)$(OMe)_2$ functionality, which can be described as a monobasic (acid) derivative of unstable orthocarbonic acid. Therefore, we explored two additional exchange processes, *iii* and *iv*, which are formally related to *i* and *ii*, but involve intramolecular proton transfer, instead of concerted exchange at the metal center. To simplify the picture, we restrained our study to purely intramolecular exchange processes, although it seems likely that proton exchange rates would be significantly enhanced in the presence of water and methanol. In principle, pathway *iii* appears a logical process because the metal-bound oxygen should be naturally a good proton acceptor. This process has the same effect as *i*, connecting **M1** and **M0** through a single, concerted transition state, **TSM10'**. The second type of intramolecular proton transfer, *iv*, shifts the hydroxyl proton to one of the OMe substituents. The corresponding transition state, **TSM12'**, leads to the elimination of a molecule of methanol. IRC calculations shows that the methanol formed in *iv* remains linked through a hydrogen bond in **M2'** but nothing similar was noted in *iii*. From **M2'**, the pathway to the **M3** only takes one more step, dissociation of the weakly bound methanol molecule. Before considering the whole reaction mechanism, it is appropriate devoting a closer look to the energies of the transition states and to the species directly connected to the intermediates **M1**, presented in Figure 5.

Only one of the four transition states, **TSM10'**, lies at a sufficiently high energy to rule out any significant contribution to the reaction mechanism, either for M=Ni or Pd. In consequence, the attack of the hydroxide complexes on the carbonyl is defined by a single process leading to **TSM10**, and then to **M1**. Two alternative processes open at this point, either intramolecular M–O bond exchange (**TSM12**) or concerted

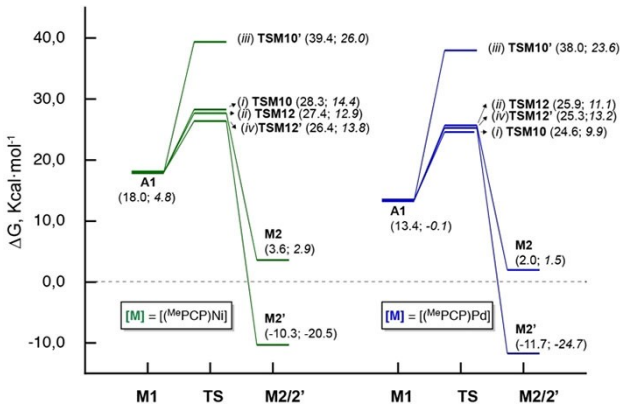

Figure 5. Free energy plot showing the relative energies of the species involved in processes *i-iv*. Free energies (computed at 298 K) and electronic energies (ZPE and solvent corrected) are explicitly shown in plain and italic fonts (in Kcal·mol^{-1}) are all relative to **M0**.

methanol elimination (**TSM12'**), with a difference of barely one Kcal·mol^{-1}. Either for Ni or Pd, **TMS12'** has lower energy than **TMS12**, which leads to the same least energy pathway, the one highlighted in Scheme 5. An interesting effect of the different nucleophilicity of the nickel and palladium hydroxides is the different role of the initial attack, since, for M=Ni, **TSM10** is higher in energy than **TSM12** and **TSM12'** whereas the opposite is true for M=Pd. In other words, for the less nucleophilic nickel hydroxide, the initial attack is rate-determining and irreversible, whereas for Pd, the decomposition of **M1** (either through **TSM12** or **TSM12'**), is slower than its formation (**TSM10**) which might even be reversible. However, the energy differences between **TMS10** and **TMS12'** are very small and, as mentioned above, the presence of water may provide a faster route for the decomposition of **M1**. Yet, the results of our calculation for the $B_{Ac}2$ mechanism are in reasonably good agreement with our experimental results. Considering the least energy pathway shown in Scheme 5, the overall energy barriers at 298 K (25 °C) would be 28.3 and 25.3 Kcal·mol^{-1} for Ni (**TSM10-Ni**) and Pd (**TSM12'-Pd**), respectively. To match more closely the experimental conditions, the calculation for M=Ni was repeated applying the thermal and solvent corrections at 323 K (50 °C). This had no impact on the general profile but slightly raised the overall energy barrier up to 29.5 Kcal·mol^{-1}. These results compare reasonably well with the data given in Figure 3 (Ni, 27.3 and Pd 22.8 Kcal·mol^{-1}). Note the similar deviation for Ni and Pd, $\approx +2$ Kcal·mol^{-1}.

As discussed before, comparing the energy barriers for the attack of the hydroxide on the carbonyl functionality of DMC (**TSM10**) provides an independent assessment of the nucleophilicithy of the Ni and Pd hydroxides. In contrast with benzaldehyde, the Ni–Pd differential in terms of free energy $\Delta\Delta G^{\ddagger}_{(Ni\text{-}Pd)}$ (3.7 Kcal/mol^{-1}) and the temperature-independent $\Delta\Delta E_{(Ni\text{-}Pd)}$ (4.5 Kcal·mol^{-1}) give similar values. The latter matches the above-mentioned difference of strength of the [Ni]–OH and [Pd]–OH bonds, suggesting that steric effects play only a minor role in the nucleophilic attack on a small molecule like DMC. This conclusion is supported by the negligible contribution of

the ZPE corrections to $\Delta\Delta E_{(Ni\text{-}Pd)}$ for **TMS10** (Table S7). Thus, in the case of DMC, the lower nucleophilicity of the nickel *vs.* the palladium hydroxide could be attributed almost entirely to a ground state effect, the stronger Ni–OH bond relative to its palladium counterpart.

Figure 6 provides global view of the free energy profiles of the $B_{Ac}2$ and $B_{Al}2$ mechanisms (the former showing only the least energy pathway). The $B_{Al}2$ mechanism begins with **TSM04**, a typical S_N2-type transition state whereby a Me^+ group is transferred from DMC to the coordinated hydroxide. The transferred methyl ends up as a neutral methanol ligand in **M4**. In a typical medium-low polarity solvent like DMC, charge separation is severely penalized. Therefore, **M4** exists briefly as tight ion-pairs that readily collapse into **M3** through the strongly exergonic displacement of coordinated methanol by the methylcarbonate anion. For both Ni and Pd, the somewhat higher energy barriers met in the $B_{Al}2$ pathway can be also attributed to the polar nature of **TSM04**, therefore $B_{Ac}2$ should be preferred. However, since the difference is small (only 0.8 Kcal·mol^{-1} for Ni, and 1.9 in the case of Pd), it cannot be excluded that, under different conditions, the $B_{Al}2$ mechanism could become prevalent (e.g., highly polar solvents or higher temperature). In fact, the calculation suggests that, even in neat DMC as solvent, a fraction of the [M]–OCO_2Me product (as much as 20% for M=Ni) could be produced through the $B_{Al}2$ route. Interestingly, the relative nucleophilicity of the Ni and Pd hydroxides in the S_N2-type $B_{Al}2$ pathway is significantly smaller than in the $B_{Ac}2$ mechanism. Even in terms of $\Delta\Delta E_{(Ni\text{-}Pd)}$, the difference between the barriers corresponding to **TSM04** is only 2.3 kcal·mol^{-1} (recall the value 4.5 Kcal·mol^{-1} for **TSM12**), which might appear incongruent with the previous discussion on the relative strengths of the [M]–OH bond. This is mostly due to the different solvent stabilization effect on the transition states. Accordingly, a re-evaluation of the relative energies of the transition states in the gas phase, gave a larger energy difference ($\Delta\Delta E_{(Ni\text{-}Pd)}$ = 3.7 Kcal·mol^{-1}) more consistent with the [M]–OH bond strengths in the Ni and Pd hydroxides.

As foreseen, examination of the picture provided by competing $B_{Ac}2$ and $B_{Al}2$ in the reverse direction produces some interesting pieces of insight relative to direct DMC synthesis from methanol and CO_2. It should be mentioned beforehand that the experimental conditions applied to promote DMC synthesis differ in two important conditions from those applied in our study of their cleavage by the Ni and Pd hydroxides. One of them is the presence of a large amount of CO_2 (usually as a pressurized atmosphere), and the second is that the solvent for such reactions is usually moist methanol (recall that water is one of the products of the synthesis), and not anhydrous DMC. Under CO_2, methoxide [M]–OMe and hydroxide [M]–OH complexes are immediately trapped as the corresponding methylcarbonate [M]–OCOOMe. While the latter is a required condition for catalysis, sequestration of the methoxide intermediates rules out the $B_{Ac}2$ branch that crosses through **M2** and **TS12**. This route would be also disfavored in moist methanol because water catalyzes the decomposition of monomethyl carbonate. Gratifyingly, neither CO_2 or water should pose an obstacle for the $B_{Ac}2$ mechanism through **M2'** or **TSM12'**. Since this mechanism offers the least energy route, the main conclusions from our calculation hold under CO_2 and methanol, leaving the scenario presented in Figure 6 as a realistic description of the actual situation during DMC synthesis. Moreover, the increased polarity and solvation capacity of methanol could have a beneficial effect, lowering the energy of some of the barriers, particularly along the ionic pathway provided by the $B_{Al}2$ route.

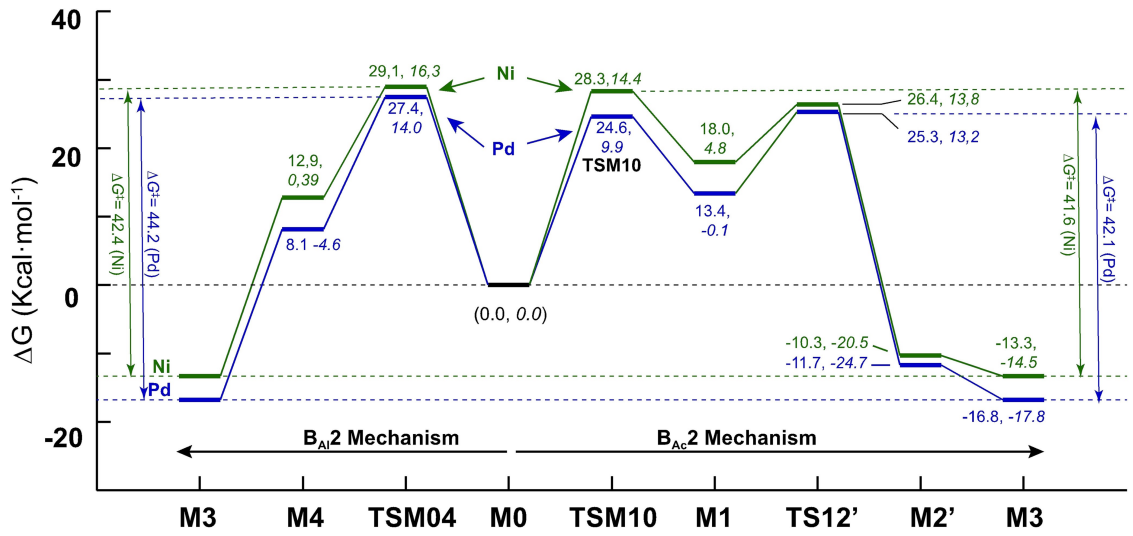

Figure 6. Free energy profile (PBE/(CPCM)/6-31G*//PBED3(CPCM)//6-311++G(3df,2p)) (solv.=DMC) for the alternative mechanisms shown in Scheme 5. Free energies (ΔG° or $\Delta G^{\ddagger}$, computed at 298 K) and electronic energies (ZPE and solvent corrected) are explicitly shown in plain and italic fonts (in Kcal·mol^{-1}) with regard to M0, and the mechanism type ($B_{Ac}2$ or $B_{Al}2$) is indicated with arrows at the bottom. Feasible reaction pathways are denoted by solid lines connecting stationary points, and dotted lines represent less favored routes that can be ruled out. Global free energy barriers are indicated by solid, doubly-headed arrows in the foremost right and left sides of the plot.

Full Papers
doi.org/10.1002/ejic.202100400

Independently of the mechanism, the **M3**→**M0** process is thermodynamically uphill both for Ni and Pd ($\Delta G^{\circ} = +13.3$ and $+16.8$ Kcal·mol^{-1}, respectively). The equilibrium constants for such process would be very small, but probably not so much as to imply that this reaction is thermodynamically locked (particularly, the equilibrium would be shifted using methanol as the solvent). Rather, the reason for the failure of the [(^{iPr}PCP)MOCO$_2$Me] complexes to produce some amount of DMC is kinetic in origin. The double-sided arrows in the right side of Figure 6 indicate the free energy barriers associated to the reverse $B_{Ac}2$ mechanism. These are too high, but remarkably similar for Ni and Pd: 41.6 and 42.1 Kcal·mol^{-1}, respectively. Barriers over 40 Kcal·mol^{-1} are effectively inaccessible at moderate temperatures. Applying heat to overcome the energy barrier would be detrimental, as concentration of DMC in equilibrium with methanol and CO_2 is expected to decrease sharply with the temperature.[18] Our calculations indicate that the alternative route through the reverse $B_{Al}2$ mechanism has a slightly higher energy barrier than the $B_{Al}2$ route, but this could be reduced by increasing the solvent polarity, due to the stabilization of the ion pair **M04**. Interestingly, the reverse $B_{Al}2$ path is reminiscent of an ionic mechanism that we suggested before for the reaction of the methylcarbonate [(^{iPr}PCP)M(OCO$_2$Me)] with MeI, on the basis of experimental kinetic data.[15b] This mechanism included the formation the ion pair {(^{iPr}PCP)M←IMe]$^+$ [O$_2$CMe]$^-$} (akin to **M4**) prior to the backside attack of the methylcarbonate anion on the activated iodomethane molecule. Unfortunately, the experimental evidence that we have collected thus far demonstrates that using methanol as solvent is still not enough to induce DMC synthesis with the pincer hydroxide complexes.[10,15b]

As can be readily perceived in Figure 6, the main contributor to the large kinetic barrier met in the reverse pathway $B_{Ac}2$ is the unfavorable nature of the methanol addition step (**M2**→**TSM12'**). Therefore, examination of the corresponding transition states, provides further insight on the ultimate causes of the irreversibility of the reaction of DMC with pincer hydroxide complexes. Shown in Figure 7 is a representation of the optimized geometries for **TMS12'** (Ni,Pd), with a simplified atom numbering scheme to facilitate the discussion.

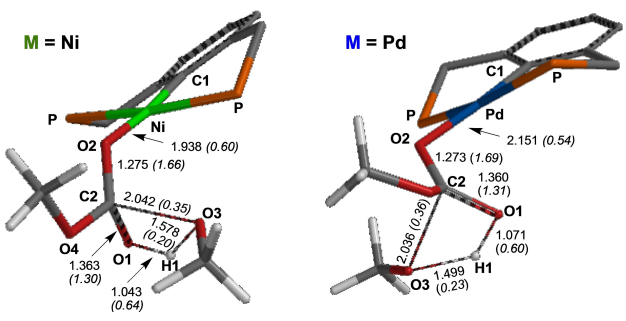

Figure 7. Optimized geometries (PBE(CPCM)/6-31G* of **TSM12** for M=Ni (left) and Pd (right), showing some relevant bond lengths and bond orders (Löwdin, in parenthesis). For clarity, all non-essential hydrogen atoms and P methyl substituents have been omitted.

Because transition states **TMS12'** describe a ligand-centered rearrangement of the orthocarbonate moiety, their energies and main geometric parameters are very similar for M=Ni and Pd. According to Hammond's Postulate, transition states should resemble more closely the reagent or the product, depending on which is higher energy. In consequence it would be expected that **TSM12'** would be much more akin to **M1** than to **M2'**. However, the feature that immediately catches the attention in both the Ni and Pd TS's is the visibly long C2···O3 bond, that is nearly broken in the transition state (Löwdin bond orders are *ca.* 0.35 for M=Ni or Pd). Furthermore, the nearly flat configuration of the O2–C2(O1)–O4 fragment, confirms that this part of **TSM12'** resembles much more to **M2'** than **M1**, in apparent contradiction with Hammond's Postulate. Yet, there is an important difference between the geometries of **TSM12'** and **M2'**: The H1 atom, whose transfer defines the internal reaction coordinate, is still more strongly bound to the carbonyl O1 (Löwdin bond order *ca.*0.62) than to O3 (*ca.* 0.21). This feature is revealing the true nature of this transition state, which is a proton transfer, rather than a nucleophilic attack of methanol on the carbonyl. Looking again in the uphill direction (**M2'**→**M1**), H^+ transfer from O3 to O1 looks as an activation required *prior* to C2–O3 bond formation. This enhances the electrophilicity of the otherwise unreactive ester carbonyl that, in this way, becomes ready to receive nucleophilic attack by the negatively polarized methoxide (much like in a general acid-catalyzed reaction). Most of the C2–O3 bond formation proceeds on going from **TSM12'** to **M1**. The prohibitive size of the energy barriers for the **M2**→**M1** processes reflect the fact that both partners in the proton transfer (the methylcarbonate complexes and methanol) are very weak bases and acid, respectively.[41]

To conclude the analysis of our computational model, it is worthwhile a comment on the reasons that make the "tetrahedral adducts" like **A1** or **M1** such elusive and thermally unstable species. The ligand bound to the metal in these species is a particular type of alkoxide, bearing electron-withdrawing substituents at the carbon atom: OH, OMe (**M1**) or OH, Ph and H (**A1**). On a general basis, alkoxide complexes of the type [(^{iPr}PCP)M(OR)] with common R groups (methoxide, ethoxide, etc.) are all reasonably stable in solution, particularly for M=Ni.[13] In line with our experimental findings, the energy barriers computed for β-H elimination in **A1** are significantly lower than those that have been computed or experimentally determined for those "normal" alkoxides. Intramolecular methanol elimination from **M1** has also a rather low activation energy. Thus, it is pertinent asking how the electronegative substituents cause the instability of this particular type of alkoxides. Close examination of the optimized geometries of the "tetrahedral adducts" reveals remarkably short [M]O–C bond distances. The effect is somewhat more pronounced for complexes **M1**, where the optimized [M]C–O bond lengths are 1.378 Å for M=Ni and 1.358 Å for Pd. These are intermediate between typical single and double carbon-oxygen bonds computed at the same level of the theory (e.g., terminal O–Me bonds in the same models are 1.425 Å in average, and the computed C=O bond length for DMC is 1.224 Å). The bond orders (Löwdin, ≈1.45) for the O–C bonds

in the "tetrahedral adducts" confirm that these are intermediate between simple and double in comparison with typical O–CH_3 (1.10) or O=C of DMC (2.06). Shortened α-O–C bonds are frequently observed in the experimental X-ray structures of many "normal" metal-alkoxides including Ni and Pd pincer moieties, whose IR spectra also reveal a significant hypsochromic shift of the ν(C–O) absorption, that supports a higher bond order in comparison with the corresponding alcohols. Unfortunately, the bond shortening is underestimated by DFT calculations,[10,13] although the unsophisticated combination PBE/6-31G* reproduces well the experimental O–C frequencies.[13] The origin of the effect did not appear clearly in the calculation outputs, but the short C–O bonds in **A1** and **M1** prompted us to revise the shapes of molecular orbitals (MO) in these compounds. Figure 8 shows the optimized structure of **M1**-Ni, with the energies of their frontier orbitals (a similar plot is shown in Figure S12 for **M1-Pd**). There are a couple of high energy occupied MOs that show significant contributions of π-symmetry orbitals. These extend over the O2–C2 vector (marked with hollow arrows), contributing to raise the net bond order. The situation is very similar for **M1-Pd** (except that in this case, the involved orbitals are the HOMO and HOMO-2). The strengthening of the O(2)–C(2) bond can be viewed as the result of the interaction of the *p*-π ("lone pairs") localized on the O2 atom with combinations of the antibonding MO associated to the σ bonds C(2)–OH and C(2)–OMe. In agreement with this interpretation, the calculation indicates that the latter bonds are slightly longer (1.44–1.45 Å) and weaker (bond orders ≈1.05) than typical single O–Me bonds (see above). The reason why this effect is more clearly observed in these species than in simpler alkoxocomplexes analyzed in our previous work, is doubtless the lower energy and better electron-acceptor properties of the α-carbon (C2) when this is bound to electron-withdrawing groups. Interestingly, both for Ni and Pd, the MO's involved also display evident antibonding interactions between the O2 "lone pairs" *p*-π orbital and the metal-centered orbitals (prevailingly d_{xy} and d_{xz} in character). These may be raising the energy of the nonboning oxygen lone pairs, thus enhancing their donor capacity. A similar "push-pull" mechanism based was proposed by Caulton to explain the IR frequencies of carbonyl ligands in *trans* to π-donor ligands.[42] With independence of the importance of the latter effect, it seems that the strengthening of the [M]–OC bond is gained at the expenses of the σ-C–OH and/or C–OMe bonds, which become weakened and more prone to cleavage. In the case of **A1** intermediates, a similar effect weakens the C2–H bond and lowers the energy barrier for β-H elimination. The weakening of the β C–H bond is readily perceived in the optimized geometries for both Ni and Pd **A1** adducts, where the C2–H bond is longer (*ca.*1.12 Å) and weaker than usual (bond order ≈0.85). The same explanation holds for the more common alkoxides [(^{iPr}PCP)MOCH$_2$R], but lacking electron-withdrawing groups, the labilizing effect of the oxygen is less pronounced. It seems likely that the "push-pull" effect of the filled metal *d*-orbitals may contribute to the destabilization of this class of complexes and, in general, of the late transition metal alkoxides. However, it should be stressed that the ability of the alkoxo oxygen to labilize the vicine β-H atoms is primarily due to the excess of electron density induced by the strong polarization of the M–O bond.

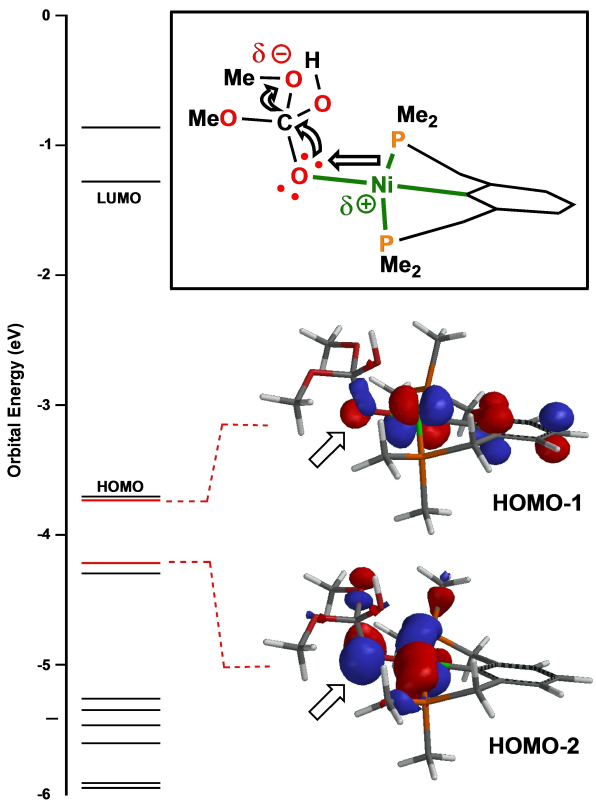

Figure 8. Molecular orbitals HOMO-1 and HOMO-2 as calculated for the **M1-Ni** intermediate. The position of both orbitals is shown in the general MO energy diagram. The hollow arrows point to π-bond lobes along the C–O bond. A simplified molecular diagram is shown in the top, showing conventional electron flow arrows representing the "push-pull" effect in the MO–C(OH)(OMe)$_2$ moiety (see discussion).

Conclusion

This investigation has conclusively demonstrated that the cleavage of dimethyl carbonate (DMC) by the hydroxide complexes [(^{iPr}PCP)M(OH)] (M=Ni or Pd) is an irreversible process. This precludes a potential of such monomeric hydroxides as catalysts for DMC synthesis from methanol and CO_2. Both pincer hydroxides (M=Ni, Pd) are competent nucleophiles towards other organic electrophiles, like PhCHO or isocyanides, but the Pd hydroxide is a significantly stronger nucleophile than its Ni analog. The outcome of the reactions with electrophiles like PhCHO and DMC can be rationalized assuming initial addition of the [M]–OH linkage across carbonyl functionality. The resulting "tetrahedral adducts" are unstable intermediates, whose decomposition irreversibly leads to the final products. One such adducts was unambiguously detected in equilibrium with mixtures of [Pd]–OH with PhCHO at −30 °C. In general, initial addition of the Ni or Pd hydroxides to PhCHO or DMC is thermodynamically disfavored, but the overall reaction is driven by strongly exothermic steps triggered by the decomposition of

the tetrahedral intermediates. The cleavage of DMC is slowed down by side equilibria that partially sequester the hydroxide reagent as binuclear carbonate, but given long enough reaction times or high temperatures, it proceeds cleanly to completion, quantitatively yielding the methylcarbonate [(^{iPr}PCP)M(OCO_2Me)] and methanol as the only final products.

DFT modeling reproduces the main reactivity trends and predicts energy barriers consistent with their experimental values, therefore the analysis of these models provides deep insight on their mechanisms. The calculations support the ability of both hydroxides to irreversibly cleave DMC. Our calculations indicate that the reaction of Ni or Pd hydroxides with DMC favors a $B_{Ac}2$ mechanism over the $B_{Al}2$. The cleavage of DMC owes its irreversibility to kinetic rather than thermodynamic causes. Overall, the balance for the cleavage is clearly exergonic (by *ca.* 13–16 Kcal·mol^{-1}) but not enough to prevent its reverse in a hypothetic catalytic cycle. However, for both Ni and Pd, high energy barriers over 40 Kcal·mol^{-1} prevent the reverse processes to take place to any significant extent. However, our calculations suggest that the $B_{Al}2$ route could provide a lower energy pathway in strongly polar solvents, or with alcohols bearing a weaker HO–C bond. Analyses of the different contributions to the energy barriers for the attack of the Ni and Pd hydroxides on the carbonyl of PhCHO and DMC suggest that the lower nucleophilicity of the nickel hydroxide stems from the smaller size of the Ni(II) center, as compared to Pd(II). The effect is mainly exerted at the ground state of the hydroxide, as a consequence of the stabilization of the [Ni]–OH bond (due to the stronger ionic contribution), and, also in the destabilization of the addition transition state, by the crowding caused by smaller size of the coordination sphere of Ni.

In addition, our DFT model provides also revealing insights on the causes of the thermal instability of the "tetrahedral adducts", that can be extended to the general issue of the low stability of the alkoxide complexes of late transition metals. The optimized structures of these intermediates show unusually short MO–C, caused by the transfer of electron density from the alkoxide oxygen into empty antibonding MOs associated to the substituents attached to the carbon atom. This transfer mitigates the excess of electric charge localized on the alkoxide oxygen atom, at the expense of the strength of the β-C–OR and β-C–H. In turn, the latter become labile and chemically active. This phenomenon is enhanced by the partially ionic nature of the M–O bonds, and the lack of empty orbitals at the Ni or Pd centres of the adequate symmetry to accept the excess of negative charge from the alkoxide ligand. The shapes of the frontier MO's clearly show that filled-filled π *p-d* repulsions further contribute to the destabilization of the electron density on the metal-bonded O atom, but it is not clear to which point this is a significant contributor to the electron flow. The same causes are responsible for the high reactivity of late transition metal alkoxides, in contrast to similar derivatives of the early transition metals with empty *d* orbitals that can accept π-bond donation from the alkoxide ligand.

Experimental Section

General Considerations

All operations were carried out under oxygen free nitrogen atmosphere using conventional Schlenk techniques or a nitrogen-filled glove box. Solvents were rigorously dried and degassed before use. Microanalyses were performed by the Analytical Service of the Instituto de Investigaciones Químicas. IR spectra were recorded on a Bruker Vector 22 spectrophotometer. NMR spectra were recorded on Bruker DPX-300, or DRX-400 spectrometers. Chemical shifts (δ) are in ppm. Solvents were used as internal standards for the reference of ^{1}H and ^{13}C spectra, but chemical shifts are referenced with respect to TMS. ^{31}P spectra are reported with respect to external H_3PO_4. For reaction monitoring purposes, a glass capillary containing a solution of PPh_3 in C_6D_6 was used as external reference. This procedure also allows using normal, non-deuterated solvents like THF. In this case, the deuterium signal from the external standard was used as the lock signal. Assignment of signals were assisted by combined one-dimensional (gated-^{13}C) and two dimensional 2D homonuclear ^{1}H-^{1}H COSY, phase sensitive NOESY, and heteronuclear ^{13}C-^{1}H HSQC and HMBC heterocorrelations. Abbreviations for multiplicities are as usual and the letter "v" denote "virtual". Apparent constants for virtual couplings are marked with asterisk (*). GC and GC-MS analyses were carried out in a Hewlett-Packard 6890 series (equipped with a HP1 capillary column and TCD detector) or ThermoQuest Trace GC 200 series (equipped with a HP-Innowax capillary column and Automass Multi MS detector). Complexes [(^{iPr}PCP)M(OH)] (M=Ni, Pd) were prepared as previously described.[11] Acetone, acetophenone, *t*-BuNC, benzoic, p-nitrobenzoic, p-dimethylaminobenzoic acids were purchased from commercial sources, and used as received. Commercial DMC was fractionally distilled under nitrogen atmosphere (slightly over 1 atm), removing the distillation head and tail fractions, and stored in a gas-tight glass ampule under nitrogen atmosphere.

Reaction of [(^{iPr}PCP)NiOH] with acetophenone. *In situ* identification of the enolate complex [(^{iPr}PCP)NiOC(=CH_2)Ph]. To a solution of 30 mg (0.073 mmol) of (^{iPr}PCP)NiOH in 1 mL of C_6D_6 were added 17 µL of acetophenone (0.14 mmol, 2 equiv.). The ^{31}P{^{1}H} spectrum of the mixture showed two signals for the starting material (55.2) and the product (54.2 ppm) in *ca.* 10:2 intensity ratio. The mixture was stirred for 6 h with 5 Å molecular sieves. At this point, the rate of the starting hydroxide to the enolate was 30:70. ^{1}H NMR (300 MHz, C_6D_6, 25 °C) δ = 1.04 (dtv, $^3J_{HH} \approx {}^*J_{HP} \approx 6.9$ Hz, 12 H, CH*Me*Me), 1.32 (dtv, $^3J_{HH} \approx {}^*J_{HP} \approx 7.3$ Hz, 12 H, CHMe*Me*), 1.97 (m, 4 H, C*H*Me$_2$), 2.99 (tv, $^*J_{HP}$ = 4.2 Hz, 4 H, CH_2 (^{iPr}PCP)), 4.55 (s, 1 H, =C*H*H), 4.76 (s, 1 H, =CH*H*), 6.83 (d, $^3J_{HH}$ = 7.3 Hz, 2 H, *m*-CH_{arom} (^{iPr}PCP)), 7.13 (m, 1 H, *p*-CH_{arom} (Ph)), 7.28 (t, $^3J_{HH}$ = 7.3 Hz, 1 H, *p*-CH_{arom} (^{iPr}PCP)), 7.30 (t, $^3J_{HH}$ = 7.6 Hz, 2 H, *m*-CH_{arom} (Ph)), 8.10 (d, $^3J_{HH}$ = 7.7 Hz, 2 H, *o*-CH_{arom} (Ph)) ppm. ^{13}C{^{1}H} (75 MHz, C_6D_6, 25 °C) δ = 17.8 (CH*Me*Me), 18.5 (CHMe*Me*), 23.8 (tv, $^*J_{CP}$ = 9.7 Hz, *C*HMe$_2$), 31.7 (tv, $^*J_{CP}$ = 12.9 Hz, *C*H_2 (^{iPr}PCP)), 78.4 (=CH_2), 121.9 (tv, $^*J_{CP}$ = 8.3 Hz, *m*-CH_{arom} (^{iPr}PCP)), 124.8 (*p*-CH_{arom} (^{iPr}PCP)), 125.6 (*o*-CH_{arom} (Ph)), 126.7 (*i*-C_{arom} (Ph)), 128.2 (*m*-CH_{arom} (Ph)), 132.3 (*p*-CH_{arom} (Ph)), 152.4 (tv, $^*J_{CP}$ = 12.9 Hz, *o*-C_{arom} (^{iPr}PCP)), 154.8 (t, $^2J_{CP}$ = 17.1 Hz, *i*-C_{arom} (^{iPr}PCP)), 166.3 (*C*=CH_2) ppm. ^{31}P{^{1}H} (121 MHz, C_6D_6, 25 °C) δ = 54.2 ppm.

Reaction of [(^{iPr}PCP)PdOH] with acetone. Synthesis of the acetonyl complex [(^{iPr}PCP)PdCH_2C(=O)CH_3]. A solution of 152 mg (0.33 mmol) of the hidroxide (^{iPr}PCP)PdOH in 20 mL of Et_2O was treated with 0.1 mL (1.36 mmol) of acetone. The mixture was stirred for 5 min at room temperature, then the solvent was evaporated under reduced pressure. The solid residue was extracted with hexane and the solution filtered. The compound was isolated as a white microcrystalline solid after concentration and cooling the

solution at −25 °C. Yield: 85 %. IR (Nujol): ν (cm^{-1}) = 1608 (ν(C=O). ^{1}H NMR (300 MHz, C_6D_6, 25 °C) δ = 0.82 (dtv, $^3J_{HH} \approx {}^*J_{HP} \approx 6.9$ Hz, 12 H, CH*Me*Me), 1.17 (dtv, $^3J_{HH} \approx {}^*J_{HP} \approx 7.3$ Hz, 12 H, CHMe*Me*), 2.20 (m, 4 H, *CH*Me$_2$), 2.24 (s, 3 H, *CH*$_3$), 2.63 (dtv, $^2J_{HP}$ = 4.5 Hz, 2 H, *CH*$_2$COCH$_3$), 2.99 (tv, $^*J_{HP}$ = 4.2 Hz, 4 H, *CH*$_2$ (^{iPr}PCP)), 7.12 (m, 3H, *CH*$_{arom}$) ppm. ^{13}C{^{1}H} (75 MHz, C_6D_6, 25 °C) δ = 17.8 (CH*Me*Me), 19.0 (tv, $^*J_{CP}$ = 2.7 Hz, CHMe*Me*), 23.3 (tv, $^*J_{CP}$ = 11.0 Hz, *C*HMe$_2$), 27.2 (tv, $^*J_{CP}$ = 6.7 Hz, *C*H$_2$COCH$_3$), 30.8 (*C*H$_3$), 36.7 (tv, $^*J_{CP}$ = 12.1 Hz, *C*H$_2$ (^{iPr}PCP)), 121.5 (tv, $^*J_{CP}$ = 10.0 Hz, *m*-*C*H$_{arom}$ (^{iPr}PCP)), 124.8 (*p*-*C*H$_{arom}$ (^{iPr}PCP)), 149.3 (tv, $^*J_{CP}$ = 10.2 Hz, *o*-*C*$_{arom}$ (^{iPr}PCP)), 170.4 (*i*-*C*$_{arom}$ (^{iPr}PCP)), 209.1 (*C*=O) ppm. ^{31}P{^{1}H} (121 MHz, C_6D_6, 25 °C) δ = 58.6 ppm. Elemental analysis for $C_{23}H_{40}OP_2Pd$ (500.9): calcd. C 55.15, H 8.05; found C 54.80, H 8.20.

Reaction of the hydroxide complexes [(^{iPr}PCP)MOH] with *t*BuNC. Syntheses of the carbamate complexes [(^{iPr}PCP)MC(=O)NH*t*Bu] (M=Ni or Pd). These compounds were prepared according to the same procedure, here we describe the method to prepare the Pd derivative: 37 μL (0.33 mmol) of *t*-BuNC were added to a solution of 150 mg (0.33 mmol) of (^{iPr}PCP)PdOH in 20 mL of THF at −80 °C. The mixture was left to reach room temperature, stirred for 1 h and then was evaporated under reduced pressure. The solid residue was extracted with hexane, and after filtration, the solution was concentrated and cooled to −30 °C. The product was separated by filtration and dried under vacuum. Yield, 181 mg, 60 %.

[(^{iPr}PCP)Ni(CONH*t*-Bu): IR (Nujol): ν (cm^{-1}) = 1547 (ν(C=O)), 3432 (ν(N–H)) . ^{1}H NMR (300 MHz, C_6D_6, 25 °C) δ = 1.00 (dtv, $^3J_{HH} \approx {}^*J_{HP} \approx 6.8$ Hz, 12 H, CH*Me*Me), 1.33 (dtv, $^3J_{HH} \approx {}^*J_{HP} \approx 7.5$ Hz, 12 H, CHMe*Me*), 1.44 (s, 9 H, *CMe*$_3$), 2.06 (m, 4 H, *CH*Me$_2$), 3.03 (tv, $^*J_{HP}$ = 3.9 Hz, 4 H, *CH*$_2$), 5.03 (sa, 1 H, N*H*), 7.14 (m, 3H, *CH*$_{arom}$) ppm. ^{13}C{^{1}H} (75 MHz, C_6D_6, 25 °C) δ = 18.2 (CH*Me*Me), 18.6 (CHMe*Me*), 24.6 (tv, $^*J_{CP}$ = 11.6 Hz, *C*HMe$_2$), 30.1 (*CMe*$_3$), 37.0 (tv, $^*J_{CP}$ = 13.9 Hz, *CH*$_2$), 50.7 (*CMe*$_3$),121.0 (tv, $^*J_{CP}$ = 8.5 Hz, *m*-*CH*$_{arom}$), 125.1 (*p*-*CH*$_{arom}$), 150.9 (tv, $^*J_{CP}$ = 12.9 Hz, *o*-*C*$_{arom}$), 174.4 (t, $^2J_{CP}$ = 12.8 Hz, *i*-*C*$_{arom}$), 210.1 (tv, $^*J_{CP}$ = 24.6 Hz, *C*=O) ppm. ^{31}P{^{1}H} (121 MHz, C_6D_6, 25 °C) δ = 59.4 ppm.

[(^{iPr}PCP)Pd(CONH*t*-Bu)]: IR (Nujol): ν (cm^{-1}) = 1558 cm^{-1}. ^{1}H NMR (300 MHz, C_6D_6, 25 °C) δ = 0.94 (dtv, $^3J_{HH} \approx {}^*J_{HP} \approx 7.2$ Hz, 12 H, CH*Me*Me), 1.27 (dtv, $^3J_{HH} \approx {}^*J_{HP} \approx 7.8$ Hz, 12 H, CHMe*Me*), 1.53 (s, 9 H, *CMe*$_3$), 2.02 (m, 4 H, *CH*Me$_2$), 3.13 (tv, $^*J_{HP}$ = 4.2 Hz, 4 H, *CH*$_2$), 4.95 (sa, 1 H, N*H*), 7.18 (m, 3H, *CH*$_{arom}$) ppm. ^{13}C{^{1}H} (75 MHz, C_6D_6, 25 °C) δ = 18.0 (CH*Me*Me), 18.7 (tv, $^*J_{CP}$ = 2.0 Hz, CHMe*Me*), 24.7 (tv, $^*J_{CP}$ = 11.2 Hz, *C*HMe$_2$), 30.2 (*CMe*$_3$), 38.2 (tv, $^*J_{CP}$ = 12.6 Hz, *CH*$_2$), 50.7 (*CMe*$_3$),121.0 (tv, $^*J_{CP}$ = 9.3 Hz, *m*-*CH*$_{arom}$), 124.8 (*p*-*CH*$_{arom}$), 149.9 (tv, $^*J_{CP}$ = 10.5 Hz, *o*-*C*$_{arom}$), 175.1 (t, $^2J_{CP}$ = 5.9 Hz, *i*-*C*$_{arom}$), 205.4 (tv, $^*J_{CP}$ = 8.3 Hz, *C*=O) ppm. ^{31}P{^{1}H} (121 MHz, C_6D_6, 25 °C) δ = 57.6 ppm.

Synthesis of [(^{iPr}PCP)M(OCO*p*-C$_6$H$_4$R) (M=Ni, Pd; R=H, NO$_2$, or NMe$_2$)]. These compounds were prepared according to the same procedure, here we describe the method to prepare the Ni benzoate (^{iPr}PCP)Ni(OCOPh): 61.1 mg (0.5 mmol) of benzoic acid were added to a solution of 207 mg (0.5 mmol) of (^{iPr}PCP)NiOH in 20 mL of THF. The mixture was stirred at room temperature for 1 h and then was taken to dryness. The solid residue was extracted with hexane, and after filtration, the solution was concentrated and cooled to −30 °C. The Ni compounds crystallized as yellow solids, and the Pd compounds as off-white or yellowish solids, in ca. 80 % yield.

(^{iPr}PCP)Ni(OCOC$_6$H$_5$). IR (Nujol): ν (cm^{-1}) = 1616 (ν(C=O)). ^{1}H NMR (300 MHz, C_6D_6, 25 °C) δ = 1.23 (dtv, $^3J_{HH} \approx {}^*J_{HP} \approx 6.9$ Hz, 12 H, CH*Me*Me), 1.37 (dtv, $^3J_{HH} \approx {}^*J_{HP} \approx 7.7$ Hz, 12 H, CHMe*Me*), 2.16 (m, 4 H, *CH*Me$_2$), 3.06 (tv, $^*J_{HP}$ = 4.1 Hz, 4 H, *CH*$_2$), 6.84 (m, 3 H, *CH*$_{arom}$ (^{iPr}PCP)), 7.32 (m, 3 H, *m*-, *p*-CH$_{arom}$ (Ph)), 7.90 (m, 2 H, *o*-*CH*$_{arom}$ (Ph)) ppm. ^{13}C{^{1}H} (75 MHz, C_6D_6, 25 °C) δ = 18.1 (CH*Me*Me), 18.8 (CHMe*Me*), 24.1 (tv, $^*J_{CP}$ = 10.0 Hz, *C*HMe$_2$), 31.3 (tv, $^*J_{CP}$ = 13.4 Hz, *CH*$_2$),122.3 (tv, $^*J_{CP}$ = 8.7 Hz, *m*-*CH*$_{arom}$ (^{iPr}PCP)), 125.3 (*p*-*CH*$_{arom}$ (^{iPr}PCP)), 127.8 (*m*-*CH*$_{arom}$ (Ph)), 129.5 (*o*-*CH*$_{arom}$ (Ph)), 129.8 (*p*-*CH*$_{arom}$ (Ph)), 137.6 (*i*-*C*$_{arom}$ (Ph)), 153.1 (tv, $^*J_{CP}$ = 12.9 Hz, *o*-*C*$_{arom}$ (^{iPr}PCP)), 153.5 (t, $^2J_{CP}$ = 17.2 Hz, *i*-*C*$_{arom}$ (^{iPr}PCP)), 170.8 (*C*=O) ppm. ^{31}P{^{1}H} (121 MHz, C_6D_6, 25 °C) δ = 57.7 ppm. Elemental analysis for $C_{27}H_{40}NiO_2P_2$ (517.3): calcd. C 62.70, H 7.79; found C 62.75, H 7.87.

[(^{iPr}PCP)Ni(OCO−*p*-C$_6$H$_4$NO$_2$)]. IR (Nujol): ν (cm^{-1}) = 1628 (ν(C=O)). ^{1}H NMR (300 MHz, C_6D_6, 25 °C) δ = 1.23 (dtv, $^3J_{HH} \approx {}^*J_{HP} \approx 7.0$ Hz, 12 H, CH*Me*Me), 1.35 (dtv, $^3J_{HH} \approx {}^*J_{HP} \approx 7.7$ Hz, 12 H, CHMe*Me*), 2.14 (m, 4 H, *CH*Me$_2$), 3.07 (tv, $^*J_{HP}$ = 4.1 Hz, 4 H, *CH*$_2$), 6.84 (m, 3 H, *CH*$_{arom}$ (^{iPr}PCP)), 8.04 (d, $^3J_{HH}$ = 8.6 Hz, 2 H, *o*-*CH*$_{arom}$ (Ph–NO$_2$)), 8.15 (d, $^3J_{HH}$ = 8.7 Hz, 2 H, *m*-*CH*$_{arom}$ (Ph–NO$_2$)), ppm. ^{13}C{^{1}H} (75 MHz, C_6D_6, 25 °C) δ = 18.1 (CH*Me*Me), 18.8 (CHMe*Me*), 24.1 (tv, $^*J_{CP}$ = 10.0 Hz, *C*HMe$_2$), 31.2 (tv, $^*J_{CP}$ = 13.5 Hz, *CH*$_2$), 122.5 (tv, $^*J_{CP}$ = 8.8 Hz, *m*-*CH*$_{arom}$ (^{iPr}PCP)), 123.2 (*m*-*CH*$_{arom}$ (Ph–NO$_2$)), 125.5 (*p*-*C*$_{arom}$ (^{iPr}PCP)), 130.4 (*o*-*CH*$_{arom}$ (Ph–NO$_2$)), 142.9 (*i*-*C*$_{arom}$ (Ph–NO$_2$)), 149.0 (*p*-*C*$_{arom}$ (Ph–NO$_2$)), 152.6 (t, $^2J_{CP}$ = 12.9 Hz, *i*-*C*$_{arom}$ (^{iPr}PCP)), 153.0 (tv, $^*J_{CP}$ = 16.9 Hz, *o*-*C*$_{arom}$ (^{iPr}PCP)), 168.9 (*C*=O) ppm. ^{31}P{^{1}H} (121 MHz, C_6D_6, 25 °C) δ = 58.1 ppm. Elemental analysis for $C_{27}H_{39}NNiO_4P_2$ (562.2): calcd. C 57.68, H 6.99, N 2.49; found C 57.79, H 6.84, N 2.66.

(^{iPr}PCP)Ni(OCO−*p*-C$_6$H$_4$NMe$_2$)]. IR (Nujol): ν (cm^{-1}) = 1602 cm^{-1} (ν(C=O)). ^{1}H NMR (300 MHz, C_6D_6, 25 °C) δ = 1.24 (dtv, $^3J_{HH} \approx {}^*J_{HP} \approx 6.9$ Hz, 12 H, CH*Me*Me), 1.37 (dtv, $^3J_{HH} \approx {}^*J_{HP} \approx 7.7$ Hz, 12 H, CHMe*Me*), 2.17 (m, 4 H, *CH*Me$_2$), 2.97 (s, 6 H, NMe$_2$), 3.05 (tv, $^*J_{HP}$ = 4.0 Hz, 4 H, *CH*$_2$), 6.82 (m, 3 H, *CH*$_{arom}$ (^{iPr}PCP)), 6.61 (d, $^3J_{HH}$ = 8.6 Hz, 2 H, *o*-*CH*$_{arom}$ (Ph–NMe$_2$)), 7.76 (d, $^3J_{HH}$ = 8.8 Hz, 2 H, *m*-*CH*$_{arom}$ (Ph–NMe$_2$)), ppm. ^{13}C{^{1}H} (75 MHz, C_6D_6, 25 °C) δ = 18.1 (CH*Me*Me), 18.8 (CHMe*Me*), 24.1 (tv, $^*J_{CP}$ = 9.9 Hz, *C*HMe$_2$), 31.4 (tv, $^*J_{CP}$ = 13.3 Hz, *CH*$_2$), 40.5 (NMe$_2$), 110.9 (*m*-*CH*$_{arom}$ (Ph–NMe$_2$)), 122.2 (tv, $^*J_{CP}$ = 8.6 Hz, *m*-*CH*$_{arom}$ (^{iPr}PCP)), 125.1 (*p*-*C*$_{arom}$ (^{iPr}PCP)), 125.8 (*i*-*C*$_{arom}$ (Ph–NMe$_2$)), 130.8 (*o*-*CH*$_{arom}$ (Ph–NMe$_2$)), 151.9 (*p*-*C*$_{arom}$ (Ph–NMe$_2$)), 153.1 (tv, $^*J_{CP}$ = 13.1 Hz, *o*-*C*$_{arom}$ (^{iPr}PCP)), 154.1 (t, $^2J_{CP}$ = 17.3 Hz, *i*-*C*$_{arom}$ (^{iPr}PCP)), 171.5 (*C*=O) ppm. ^{31}P{^{1}H} (121 MHz, C_6D_6, 25 °C) δ = 57.4 ppm. Elemental analysis for $C_{29}H_{45}NNiO_2P_2$ (560.3): calcd. C 62.16, H 8.09, N 2.50; found C 62.18, H 7.78, N 2.75.

(^{iPr}PCP)Pd(OCOC$_6$H$_5$): IR (Nujol): ν (cm^{-1}) = 1611 (ν(C=O)). ^{1}H NMR (300 MHz, C_6D_6, 25 °C) δ = 1.20 (dtv, $^3J_{HH} \approx {}^*J_{HP} \approx 7.2$ Hz, 12 H, CH*Me*Me), 1.31 (dtv, $^3J_{HH} \approx {}^*J_{HP} \approx 8.0$ Hz, 12 H, CHMe*Me*), 2.30 (m, 4 H, *CH*Me$_2$), 3.19 (tv, $^*J_{HP}$ = 4.3 Hz, 4 H, *CH*$_2$), 6.92 (t, $^3J_{HH}$ = 7.3 Hz, 1 H, *p*-*CH*$_{arom}$ (^{iPr}PCP)), 7.00 (d, $^3J_{HH}$ = 7.5 Hz, 2 H, *m*-*CH*$_{arom}$ (^{iPr}PCP)), 7.34 (m, 3 H, *m*-, *p*-CH$_{arom}$ (Ph)), 8.00 (m, 2 H, *o*-*CH*$_{arom}$ (Ph)) ppm. ^{13}C{^{1}H} (75 MHz, C_6D_6, 25 °C) δ = 18.0 (CH*Me*Me), 18.9 (CHMe*Me*), 24.8 (tv, $^*J_{CP}$ = 10.9 Hz, *C*HMe$_2$), 32.4 (tv, $^*J_{CP}$ = 11.7 Hz, *CH*$_2$),122.8 (tv, $^*J_{CP}$ = 10.5 Hz, *m*-*CH*$_{arom}$ (^{iPr}PCP)), 125.1 (*p*-*CH*$_{arom}$ (^{iPr}PCP)), 127.7 (*m*-*CH*$_{arom}$ (Ph)), 129.6 (*p*-*CH*$_{arom}$ (Ph)), 129.7 (*o*-*CH*$_{arom}$ (Ph)), 138.6 (*i*-*C*$_{arom}$ (Ph)), 151.4 (tv, $^*J_{CP}$ = 10.6 Hz, *o*-*C*$_{arom}$ (^{iPr}PCP)), 155.4 (*i*-*C*$_{arom}$ (^{iPr}PCP)), 170.8 (*C*=O) ppm. ^{31}P{^{1}H} (121 MHz, C_6D_6, 25 °C) δ = 60.4 ppm. Elemental analysis for $C_{27}H_{40}O_2P_2Pd$ (565.0): calcd. C 57.40, H 7.14; found C 57.41, H 7.26.

(^{iPr}PCP)Pd(OCO−*p*-C$_6$H$_4$NO$_2$): IR (Nujol): ν (cm^{-1}) = 1628 (ν(C=O)). ^{1}H NMR (300 MHz, C_6D_6, 25 °C) δ = 1.19 (dtv, $^3J_{HH} \approx {}^*J_{HP} \approx 7.3$ Hz, 12 H, CH*Me*Me), 1.29 (dtv, $^3J_{HH} \approx {}^*J_{HP} \approx 8.0$ Hz, 12 H, CHMe*Me*), 2.29 (m, 4 H, *CH*Me$_2$), 3.19 (tv, $^*J_{HP}$ = 4.3 Hz, 4 H, *CH*$_2$), 6.92 (t, $^3J_{HH}$ = 7.2 Hz, 1 H, *p*-*CH*$_{arom}$ (^{iPr}PCP)), 6.99 (d, $^3J_{HH}$ = 6.5 Hz, 2 H, *m*-*CH*$_{arom}$ (^{iPr}PCP)), 8.15 (m, 4 H, *CH*$_{arom}$ (Ph–NO$_2$)) ppm. ^{13}C{^{1}H} (75 MHz, C_6D_6, 25 °C) δ = 18.0 (CH*Me*Me), 18.8 (CHMe*Me*), 24.8 (tv, $^*J_{CP}$ = 10.9 Hz, *C*HMe$_2$), 32.2 (tv, $^*J_{CP}$ = 11.7 Hz, *CH*$_2$), 122.9 (tv, $^*J_{CP}$ = 10.5 Hz, *m*-*CH*$_{arom}$ (^{iPr}PCP)), 123.1 (*m*-*CH*$_{arom}$ (Ph–NO$_2$)), 125.3 (*p*-*C*$_{arom}$ (^{iPr}PCP)), 130.5 (*o*-*CH*$_{arom}$ (Ph–NO$_2$)), 144.3 (*i*-*C*$_{arom}$ (Ph–NO$_2$)), 148.9 (*p*-*C*$_{arom}$ (Ph–NO$_2$)),151.4 (tv, $^*J_{CP}$ = 10.8 Hz, *o*-*C*$_{arom}$ (^{iPr}PCP)), 154.7 (*i*-*C*$_{arom}$ (^{iPr}PCP)), 168.8 (*C*=O) ppm. ^{31}P{^{1}H} (121 MHz, C_6D_6, 25 °C) δ = 60.7 ppm. Elemental Anal. for $C_{27}H_{39}NO_4P_2Pd$ (610.0): calcd. C 53.16, H 6.44, N 2.30; found C 53.12, H 6.50, N 2.42.

([^{iPr}PCP)Pd(OCO–*p*-$C_6H_4NMe_2$): IR (Nujol): ν (cm^{-1}) = 1598 ^{1}H NMR (300 MHz, C_6D_6, 25 °C) δ = 1.20 (dtv, $^3J_{HH} \approx {}^*J_{HP} \approx 7.2$ Hz, 12 H, CH*Me*Me), 1.31 (dtv, $^3J_{HH} \approx {}^*J_{HP} \approx 8.0$ Hz, 12 H, CHMe*Me*), 2.32 (m, 4 H, C*H*Me$_2$), 2.98 (s, 6 H, N*Me*$_2$), 3.19 (tv, $^*J_{HP} = 4.3$ Hz, 4 H, C*H*$_2$), 6.65, 7.87 (AA'XX', 4 H, *o- m*-CH_{arom} (Ph–NMe$_2$)), 6.92 (t, $^3J_{HH} = 7.4$ Hz, 1 H, *p*-CH_{arom} (^{iPr}PCP)), 6.99 (d, $^3J_{HH} = 7.7$ Hz, 2 H, *m*-CH_{arom} (^{iPr}PCP)) ppm. ^{13}C{^{1}H} (75 MHz, C_6D_6, 25 °C) δ = 18.0 (CH*Me*Me), 18.9 (CHMe*Me*), 24.7 (tv, $^*J_{CP} = 10.9$ Hz, *C*HMe$_2$), 32.5 (tv, $^*J_{CP} = 11.5$ Hz, *C*H$_2$), 40.5 (N*Me*$_2$), 111.1 (*m*-CH_{arom} (Ph–NMe$_2$)), 122.8 (tv, $^*J_{CP} = 10.4$ Hz, *m*-CH_{arom} (^{iPr}PCP)), 125.0 (*p*-C$_{arom}$ (^{iPr}PCP)), 126.6 (*i*-C$_{arom}$ (Ph–NMe$_2$)), 131.1 (*o*-CH_{arom} (Ph–NMe$_2$)), 151.5 (tv, $^*J_{CP} = 10.9$ Hz, *o*-C$_{arom}$ (^{iPr}PCP)), 151.9 (*p*-C$_{arom}$ (Ph–NMe$_2$)), 155.8 (*i*-C$_{arom}$ (^{iPr}PCP)), 171.4 (C=O) ppm. ^{31}P{^{1}H} (121 MHz, C_6D_6, 25 °C) δ = 60.1 ppm. Elemental analysis for $C_{29}H_{45}NO_2P_2Pd$ (680.0): calcd. C 57.28, H 7.46, N 2.30; found C 57.29, H 7.56, N 2.47.

Simultaneous NMR and GC monitoring the reaction of [(^{iPr}PCP)PdOH] with PhCHO at room temperature. A 50 mL glass ampoule equipped with a magnetic stirrer was charged with 10 mL of a THF solution containing 23.1 mg (0.05 mmol) of the palladium hydroxide complex, and 3.9 mg of biphenyl as GC internal standard. 15.3 mL of neat benzaldehyde were added to the solution. The solution was stirred for 24 h, withdrawing aliquots of 0.7 mL at different times, which were cannula-transferred to an NMR tube containing the external reference sealed in a borosilicate glass capillary tube. After recording the ^{31}P{^{1}H} spectrum, the solution was poured in a vial in the open air and subjected to GC analyses.

Kinetics of the reactions of [(^{iPr}PCP)MOH] (M=Ni, or Pd) with neat DMC. These reactions were carried out in NMR tubes with gas-tight PTFE screw valves, containing the external reference sealed in a borosilicate glass capillary tube. In each case, an amount corresponding to 0.025 mmol of the starting complex (Ni: 10.3 mg; Pd: 11.5 mg) were dissolved in 0.6 mL of neat DMC. The samples were transferred to the NMR probe, pre-heated and stabilized at the working temperature, and the reaction progress was monitored by integration of the ^{31}P{^{1}H} resonances. Once the reaction was complete, the solution was evaporated to dryness, and dissolved in C_6D_6 to check the identity of the main products (methylcarbonate complexes, [(^{iPr}PCP)M(OCO$_2$Me)]. As reported before,[15] this procedure causes the essentially pure samples to become contaminated with some binuclear carbonate {[(^{iPr}PCP)M]$_2$(m-CO$_3$)}, but the main species was still the methylcarbonate. The identity of the resonances of the binuclear carbonate complexes in DMC was verified by comparison to the spectra of authentic samples in the same solvent and temperatures (with regard to the PPh_3 external standard). In general, the chemical shifts of every signal were quite similar to their reported values in C_6D_6. The sum of the intensities of the ^{31}P resonances was approximately constant with regard to the external standard, therefore for the kinetic calculations these were normalized giving the value 1 to the sum of all intensities. To deduce the actual values of rate constants, we used the molar concentrations of DMC, calculated using literature values of DMC at the experiment temperatures (in $Kg \cdot L^{-1}$: 25 °C, 1.063; 50 °C, 1.030).[43] The data were fit to a suitable kinetic model using the "MacKinetics" program and the results checked with the software Dynafit.[38]

Isolation of the hydrate [(^{iPr}PCP)Ni(OH)]·1/2 H_2O. Full details for the titration with water of the anhydrous hydroxide, IR data (nujol), molecular weight in solution (benzene, cryoscopy freezing point depression), elemental analysis and X-ray structure are given in the SI.

Deposition Number 2078309 (for **[Ni]OH·1/2H_2O**) contains the supplementary crystallographic data for this paper. These data are provided free of charge by the joint Cambridge Crystallographic Data Centre and Fachinformationszentrum Karlsruhe Access Structures service www.ccdc.cam.ac.uk/structures.

Computational details

All DFT calculations were performed with the Spartan'18 software package.[44] Geometry optimizations and vibrational analyses were carried out with the PBE functional and the 6–31G* for the nickel complexes and LACVP* for palladium complexes. The latter comprises the 6–31G* functions for light elements and the LANL2DZ pseudopotential for palladium. The energy gradient for criterion for geometric convergence was tightened from Spartan's default value 3×10^{-4} to 5.5×10^{-5} erg/bohr. Solvent effects were included in the optimization procedure with the CPCM implicit model, setting the Bondi-type PCM radii for Ni and Pd as 2.28 and 2.48 Å, respectively. These were estimated from X-ray diffraction structures of pincer hydroxide and alkoxide complexes, as described before.[13] The geometries of transition states were checked to have only one imaginary frequency and their identity was tested by an Internal Reaction Coordinate (IRC) calculation. Electronic (SCF) energies were refined with a single point calculation at the PBE–D3/6-311++G(3df,2p) level (SCF convergence criterion set to "HIGH"), which includes Grimme's empirical correction for dispersive forces functional, and the largest of Pople-type triple-ζ quality basis function set available in Spartan. At this level of the theory, Spartan uses the all-electron def2-TZVP basis to describe the Pd atom. Single-point calculations were accelerated using the "dual" option, which specifies that SCF convergence is achieved at the 6–311G* level, and then corrected perturbatively for the effect of additional diffuse and polarization functions. Preliminary calculations showed that the introduction of the D3 parameter during the geometry optimization only results in minor improvements of the final geometries but hampers geometry convergence, particularly for transition states. For each stationary point in the potential energy surface, free energies ($G°$) at 298 K were estimating adding the SCF electronic energies (from the higher level single point) to the Thermal and Solvent Corrections determined at the geometry optimization level of theory, namely: $G°(298\ K) = E(SCF,\ PBE\text{-}D3/6\text{-}311++G(3df,2p)) + TC\ (at\ 298\ K) + SC(298\ K)$. The same procedure was extended to different temperatures. Thermal Corrections for a given temperature were computed at the same level for which the vibrational data were available (namely, the double-ζ quality basis set used for geometry optimization) $TC(at\ T) = G°(PBE/6\text{-}31G*,\ CPCM(T)) - E(SCF)(PBE/6\text{-}31G*,\ CPCM(T))$. To compute the solvent correction, we performed an unexpensive additional gas phase single-point energy calculation on optimized geometries at the PBE/6-31*G level (*i.e.*, omitting the solvent calculation), therefore $SC(T) = E(SCF,\ PBE/6\text{-}31G*,\ CPCM(T))\text{-}E(SCF,\ PBE/6\text{-}31G*,\ gas\ phase)$. In addition to reducing the computational cost, this procedure has the advantage of computing the solvent effect at a similar level of the theory at which the CPCM model was originally parametrized.[45] CPCM calculations have their own temperature specification (independent from that of the thermal correction, but often neglected). For the calculations at temperatures different from 298 K, geometry optimization and vibrational analyses were updated with consistent use of temperature both for the thermal and solvent corrections, and single point calculations were performed over the re-optimized geometry.

Acknowledgements

This work was supported by the Spanish Research Agency (AEI), the European Union (Feder Funds) and Junta de Andalucía through projects PGC2018-095768-B-100 and PY20_0104.

Conflict of Interest

The authors declare no conflict of interest.

Keywords: Pincer complexes · Nickel · Palladium · Hydroxide complexes · Reaction mechanisms

[1] a) *Pincer Compounds: Chemistry and Applications* (Ed: D. Morales-Morales), Amsterdam, Elsevier, **2018**; b) *Pincer and Pincer-Type Complexes: Applications in Organic Synthesis and Catalysis* (Eds: K. J. Szabó, O. F. Wendt), Weinheim, Wiley-VCH, **2014**; c) *The Chemistry of Pincer Compounds* (Eds: D. Morales-Morales, C. Jensen), Amsterdam, Elsevier, **2007**; d) *Organometallic Pincer Chemistry* (Eds: G. van Koten, D. Milstein), Heidelberg, Elsevier, **2013**.

[2] a) L. S. Merz, J. Ballmann, L. H. Gade, *Eur. J. Inorg. Chem.* **2020**, 2023–2042; b) A. Singh, D. Gelman, *ACS Catal.* **2020**, *10*, 1246–1255; c) R. Arevalo, P. J. Chirik, *J. Am. Chem. Soc.* **2019**, *141*, 9106–9123; d) H. Valdés, L. González-Sebastián, D. Morales-Morales, *J. Organomet. Chem.* **2017**, *845*, 229–257; e) R. E. Andrew, L. González-Sebastián, A. B. Chaplin, *Dalton Trans.* **2016**, *45*, 1299–1305; f) S. Murugesan, K. Kirchner, *Dalton Trans.* **2016**, *45*, 416–439.

[3] See, for example: a) A. Rossin, M. Peruzzini, *Chem. Rev.* **2016**, *116*, 8848–8872; b) N. A. Eberhardt, H. Guan, *Chem. Rev.* **2016**, *116*, 8373–8426.

[4] For some discussion of the *trans* influence and labilizing effects in pincer complexes, see: a) A. J. Canty, A. Ariafard, G. van Koten, *Chem. Eur. J.* **2020**, *26*, 15629–15635; b) H.-W. Suh, T. J. Schmeier, N. Hazari, R. A. Kemp, M. K. Takase, *Organometallics* **2012**, *31*, 8225–8236; c) Y. X. Jia, X. Y. Yang, W. S. Tay, Y. Li, S. A. Pullarkat, K. Xu, H. Hirao, P. H. Leung, *Dalton Trans.* **2016**, *45*, 2095–2101; d) E. Sola, *Silicon-Based Pincers: Trans Influence and Functionality* Chapter 19 in Ref. 1a.

[5] Some representative reviews: a) H. E. Bryndza, W. Tam, *Chem. Rev.* **1988**, *88*, 1163–1188; b) M. D. Fryzuk, C. D. Montgomery, *Coord. Chem. Rev.* **1989**, *95*, 1–40; c) H. W. Roesky, S. Singh, K. K. M. Yusuff, J. A. Maguire, N. S. Hosmane, *Chem. Rev.* **2006**, *106*, 3813–3843.

[6] a) R. Jira, *Angew. Chem. Int. Ed.* **2009**, *48*, 9034–9037; *Angew. Chem.* **2009**, *121*, 9196–9199; b) A. Comas-Vives, A. Stirling, A. Lledos, G. Ujaque, *Chem. Eur. J.* **2010**, *16*, 8738–8747.

[7] a) H. Vahrenkamp, *Dalton Trans.* **2007**, 4751–4759; b) A. Dolega, *Coord. Chem. Rev.* **2010**, *254*, 916–937.

[8] A. G. Blackman, L. R. Gahan, *Z. Anorg. Allg. Chem.* **2018**, *644*, 616–629.

[9] a) H. Valdés, M. A. García-Eleno, D. Canseco-González, D. Morales-Morales, *ChemCatChem* **2018**, *10*, 3136–3172; b) V. Arora, H. Narjinari, P. G. Nandi, A. Kumar, *Dalton Trans.* **2021**, *50*, 3394–3428.

[10] L. M. Martínez-Prieto, J. Cámpora, *Isr. J. Chem.* **2020**, *60*, 373–393.

[11] J. Cámpora, P. Palma, D. del Río, E. Álvarez, *Organometallics* **2004**, *23*, 1652–1655.

[12] J. Cámpora, P. Palma, D. del Río, M. M. Conejo, E. Álvarez, *Organometallics* **2004**, *23*, 5653–5655.

[13] L. M. Martínez-Prieto, P. Palma, E. Álvarez, J. Cámpora, *Inorg. Chem.* **2017**, *56*, 13086–13099.

[14] a) C. Melero, L. M. Martinez-Prieto, P. Palma, D. del Rio, E. Alvarez, J. Campora, *Chem. Commun.* **2010**, *46*, 8851–8853; b) L. M. Martinez-Prieto, E. Avila, P. Palma, E. Alvarez, J. Cámpora, *Chem. Eur. J.* **2015**, *21*, 9833–9849.

[15] a) L. Miguel Martinez-Prieto, C. Real, E. Avila, E. Alvarez, P. Palma, J. Campora, *Eur. J. Inorg. Chem.* **2013**, *2013*, 5555–5566; b) L. M. Martinez-Prieto, P. Palma, J. Campora, *Dalton Trans.* **2019**, *48*, 1351–1366.

[16] L. M. Martínez-Prieto, Ph. D. Dissertation. *Ni and Pd Pincer Complexes: A Model for the Study of Catalytic Alcohol Carboxylation in Homogeneous Phase*, University of Seville, **2012**.

[17] a) M. Aresta, A. Dibenedetto, A. Dutta, *Catal. Today* **2017**, *281*, 345–351; b) M. Aresta, A. Dibenedetto, A. Angelini, I. Papai, *Top. Catal.* **2015**, *58*, 2–14; c) S. Huang, B. Yan, S. Wang, X. Ma, *Chem. Soc. Rev.* **2015**, *44*, 3079–3116; d) M. Aresta, A. Dibenedetto, A. Angelini, *Adv. Inorg. Chem.* **2014**, *66*, 259–288; e) T. Sakakura, K. Kohno, *Chem. Commun.* **2009**, 1312–1330.

[18] P. Tundo, M. Selva, *Acc. Chem. Res.* **2002**, *35*, 705–716.

[19] A.-A. G. Shaikh, S. Sivaram, *Chem. Rev.* **1996**, *96*, 951–976.

[20] Q. Cai, B. Lu, L. Guo, Y. Shan, *Catal. Commun.* **2009**, *10*, 605–609.

[21] See, for example: F. A. Carey, R. J. Sundberg, *Advanced Organic Chemistry, 3rd Edition. Part A, Structure and Mechanisms.* New York, Plenum Press, **1990**. pp 465–470.

[22] a) A. Arabaoui, C. Redshaw, *Polym. Chem.* **2010**, *1*, 801–826; b) D. J. Walsh, M. G. Hyatt, S. A. Miller, D. Guironnet, *ACS Catal.* **2019**, *9*, 11153–11188.

[23] a) R. Johansson, O. F. Wendt, *Organometallics* **2007**, *26*, 2426–2430; b) K. J. Jonasson, A. H. Mousa, O. F. Wendt, *Polyhedron* **2018**, *143*, 132–137; c) A. H. Mousa, J. Bendix, O. F. Wendt, *Organometallics* **2018**, *37*, 2581–2593.

[24] a) G. R. Fulmer, R. P. Muller, R. A. Kemp, K. I. Goldberg, *J. Am. Chem. Soc.* **2009**, *131*, 1346–1349; b) G. R. Fulmer, A. N. Herndon, W. Kaminsky, R. A. Kemp, K. I. Goldberg, *J. Am. Chem. Soc.* **2011**, *133*, 17713–17726; c) G. R. Fulmer, W. Kaminsky, R. A. Kemp, K. I. Goldberg, *Organometallics* **2011**, *30*, 1627–1636; d) W. D. Bailey, A. S. Phearman, L. Luconi, A. Rossin, D. G. Yakhvarov, L. D'Accolti, S. E. Flowers, W. Kaminsky, R. A. Kemp, G. Giambastiani, K. I. Goldberg, *Chem. Eur. J.* **2019**, *25*, 9920–9929.

[25] a) D. Huang, O. V. Makhlynets, L. L. Tan, S. C. Lee, E. V. Rybak-Akimova, R. H. Holm, *Proc. Nat. Acad. Sci.* **2011**, *108*, 1222–1227; b) D. Huang, O. V. Makhlynets, L. L. Tan, S. C. Lee, E. V. Rybak-Akimova, R. H. Holm, *Inorg. Chem.* **2011**, *50*, 10070–10081.

[26] T. J. Schmeier, A. Nova, N. Hazari, F. Maseras, *Chem. Eur. J.* **2012**, *18*, 6915–6927.

[27] C. Yoo, J. Kim, Y. Lee, *Organometallics* **2013**, *32*, 7195–7203.

[28] a) S. Chakraborty, P. Bhattacharya, H. G. Dai, H. R. Guan, *Acc. Chem. Res.* **2015**, *48*, 1995–2003; b) N. A. Eberhardt, N. P. N. Wellala, Y. Z. Li, J. A. Krause, H. R. Guan, *Organometallics* **2019**, *38*, 1468–1478.

[29] a) J. Cámpora, I. Matas, P. Palma, E. Álvarez, C. Graiff, A. Tiripicchio, *Organometallics* **2007**, *26*, 5712–5721; b) M. K. Samantaray, M. M. Shaikh, P. Ghosh, *Organometallics* **2009**, *28*, 2267–2275; c) M. Kujime, S. Hikichi, M. Akita, *Inorg. Chim. Acta* **2003**, *350*, 163–174.

[30] a) M. Kujime, S. Hikichi, M. Akita, *Organometallics* **2001**, *20*, 4049–4060; b) S. Kannan, A. J. James, P. R. Sharp, *Inorg. Chim. Acta* **2003**, *345*, 8–14.

[31] a) J. Cámpora, C. M. Maya, P. Palma, E. Carmona, E. Gutierrez-Puebla, C. Ruiz, *J. Am. Chem. Soc.* **2003**, *125*, 1482–1483; b) J. Cámpora, C. M. Maya, P. Palma, E. Carmona, E. Gutierrez, C. Ruiz, C. Graiff, A. Tiripicchio, *Chem. Eur. J.* **2005**, *11*, 6889–6904.

[32] a) J. Vicente, A. Arcas, J. M. Fernandez-Hernandez, D. Bautista, P. G. Jones, *Organometallics* **2005**, *24*, 2516–2527; b) K. P. Kepp, *Inorg. Chem.* **2016**, *55*, 9461–9470.

[33] S. A. Macgregor, G. W. Neave, *Organometallics* **2003**, *22*, 4547–4556.

[34] a) R. A. Michelin, R. Ros, *J. Organomet. Chem.* **1979**, *169*, C42-C44; b) W.-S. Ojo, E. Paugam, F. Y. Petillon, P. Schollhammer, J. Talarmin, K. W. Muir, *Organometallics* **2006**, *25*, 4009–4018.

[35] a) L. C. Liang, C. W. Li, P. Y. Lee, C. H. Chang, H. M. Lee, *Dalton Trans.* **2011**, *40*, 9004–9011; b) D. J. Mindiola, G. L. Hillhouse, *Chem. Commun.* **2002**, 1840–1841; c) P. L. Holland, R. A. Andersen, R. G. Bergman, *J. Am. Chem. Soc.* **1996**, *118*, 1092–1104.

[36] L. M. Martinez-Prieto, C. Melero, D. del Rio, P. Palma, J. Cámpora, E. Alvarez, *Organometallics* **2012**, *31*, 1425–1438.

[37] see Ref 21, p. 439.

[38] a) McKinetics v. 0.9.1b, by Walter Leipold III. http://members.dca.net./leipold/mk/mk091.html; b) The results were checked with DynaFit v. 4.05.103 (Biokin, Ltd).

[39] a) Y. Minenkov, A. Singstad, G. Occhipinti, V. R. Jensen, *Dalton Trans.* **2012**, *41*, 5526–5541; b) Y. Minenkov, E. Chermak, L. Cavallo, *J. Chem. Theory Comput.* **2016**, *12*, 1542–1560; c) S. Boonseng, G. W. Roffe, J. Spencer, H. Cox, *Dalton Trans.* **2015**, *44*, 7570–7577; d) M. Poor Kalhor, H. Chermette, S. Chambrey, D. Ballivet-Tkatchenko, *Phys. Chem. Chem. Phys.* **2011**, *13*, 2401–2408; e) See M. Swart's "DFT poll" (http://www.marcelswart.eu/dft-poll/), where PBE has remained within the first 4 positions for over the last 10 years.

[40] a) A. Dibenedetto, M. Aresta, P. Giannoccaro, C. Pastore, I. Papai, G. Schubert, *Eur. J. Inorg. Chem.* **2006**, 908–913; b) A. Y. Samuilov, Y. D. Samuilov, *Theor. Chem. Acc.* **2019**, *138*. DOI: 10.1007/s00214-018-2411–0.

[41] Note that the hypothetical route through **TSM12** poses an even more radical version of this problem, since the formation of **M2** is an acid-

base equilibrium involving the protonation of a methylcarbonate complex by methanol to generate methylcarbonic acid and a methoxide complex.

[42] a) K. G. Caulton, *New J. Chem.* **1994**, *18*, 25–41; b) J. T. Poulton, M. P. Sigalas, K. Folting, W. E. Streib, O. Eisenstein, K. G. Caulton, *Inorg. Chem.* **1994**, *33*, 1476–1485.

[43] E. Romano, J. L. Trenzado, E. Gonzalez, J. S. Matos, L. Segade, E. Jimenez, *Fluid Phase Equilib.* **2003**, *211*, 219–240.

[44] *Spartan'18*, Wavefuntion, Inc. Irvine, CA, USA. Version 1.4.4., 2019.

[45] J. Ho, A. Klamt, M. L. Coote, *J. Phys. Chem. A* **2010**, *114*, 13442–13444.

Manuscript received: May 10, 2021
Revised manuscript received: June 18, 2021
Accepted manuscript online: June 23, 2021